2dF Galaxy Redshift Survey

Summary

The 2dF Galaxy Redshift Survey (http://www.mso.anu.edu.au/2dFGRS/) is a major spectroscopic survey taking full advantage of the unique capabilities of the 2dF facility built by the Anglo-Australian Observatory. The 2dFGRS is integrated with the 2dFQSO survey.

Main properties

- 4 m telescope located in Australia
- Survey period: 1999-2002
- NGP field, SGP field, random fields. Based on the APM angular survey.
- Up to 400 spectra per shot: multi-target 2^{o} spectrograph
- Photometry in b_J filter

Final Data Release (June 2003)

- ~1500 sq. deg., ~4% of celestial sphere
- 245 591 galaxies, $14.0<b_J<19.45$, $z<0.3$
- $\sim 2.5 \cdot 10^4$ quasars, $18.25<b_J<20.85$, $0.5<z<2.5$

Survey map

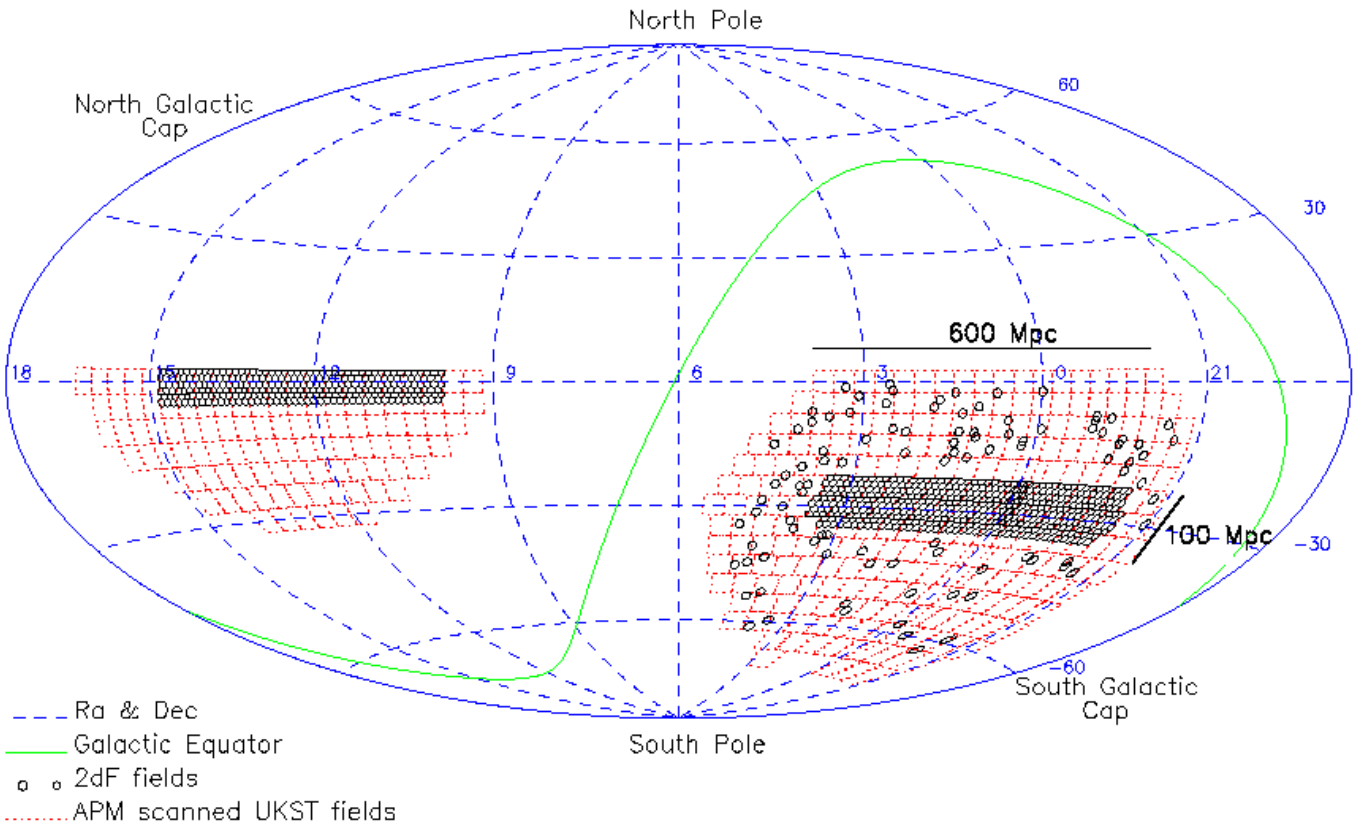

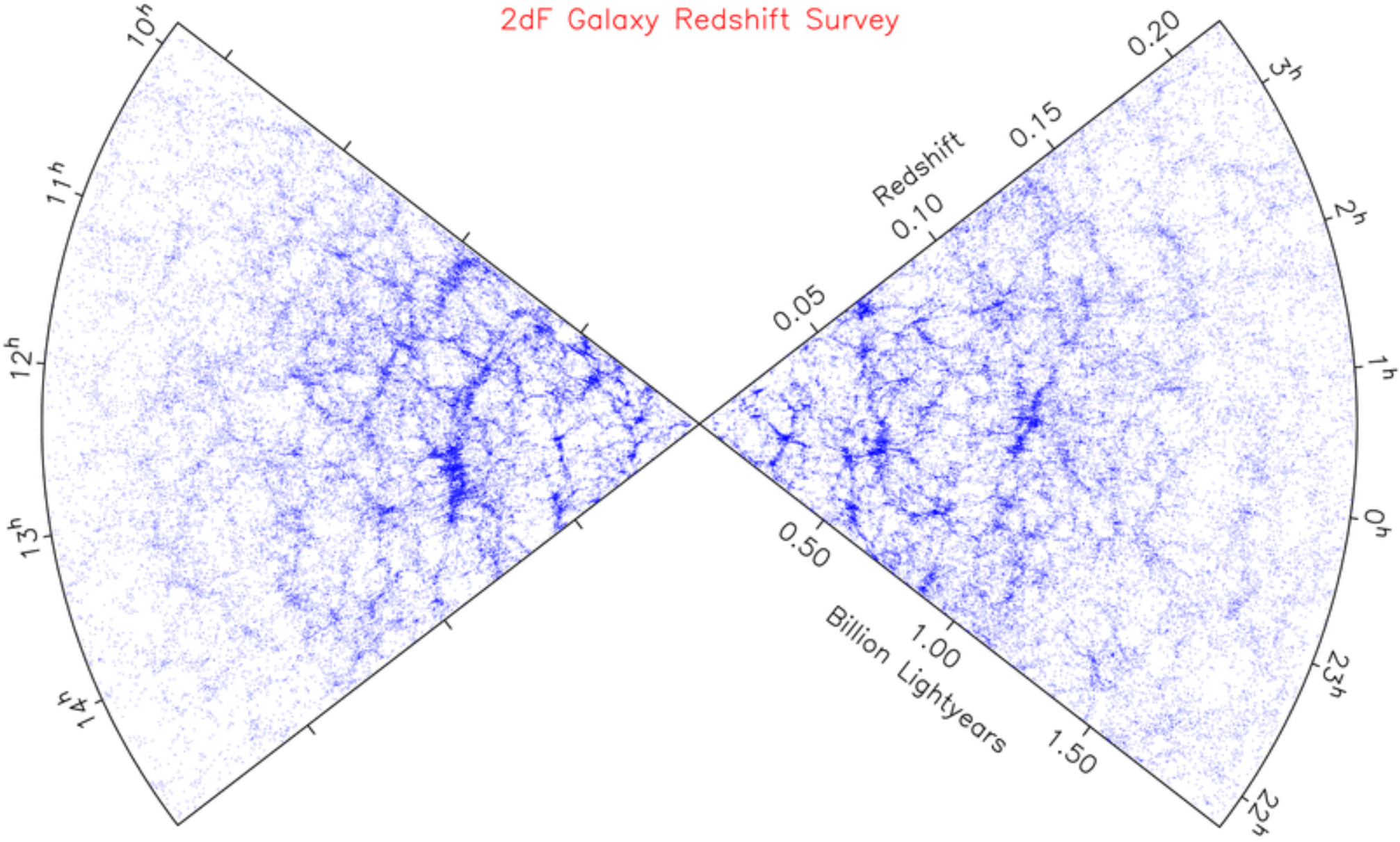
2dF Galaxy Redshift Survey
10h
11h
12h
13h
14h
Redshift
0.05
0.10
0.15
0.20
0.50
1.00
1.50
Billion Lightyears
3h
2h
1h
0h
23h
22h

Sloan Digital Sky Survey

Summary

Simply put, the Sloan Digital Sky Survey (http://www.sdss.org/) is the most ambitious astronomical survey project ever undertaken. The survey will map in detail one-quarter of the entire sky, determining the positions and absolute brightnesses of more than 100 million celestial objects. It will also measure the distances to more than a million galaxies and quasars.

Main properties

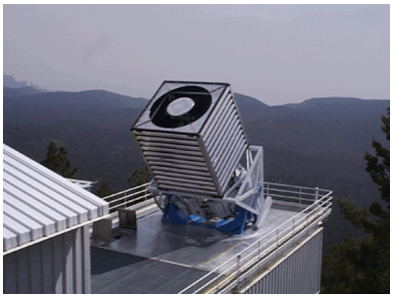

- 2.5 m dedicated telescope at Apache Point Observatory, Mexico
- Survey period: 2000-2008 (and SDSS I & II)
- 640 spectra per shot: multi-target 1.5^{o} spectrograph
- 5-band photometry: u, g, r, i, z
- EDR, DR1, DR2, ..., DR8 (and SDSS III)

Target results

- ¼ of the overall sky (π)
- 1 000 000 galaxy spectra
- 100 000 QSO spectra
- more than 100 million photometrical objects

Data Release 6 (July 2007)

- 287 million unique objects (photometry)
- Spectroscopic area: 7425 sq. deg.
- 790,860 Galaxies: MG (z<0.2, r<17.77), LRG (z<0.6)
- 90,108 Quasars (z <2.3, i<19.1)
- 13,539 Quasars (z >2.3, i<20.2)

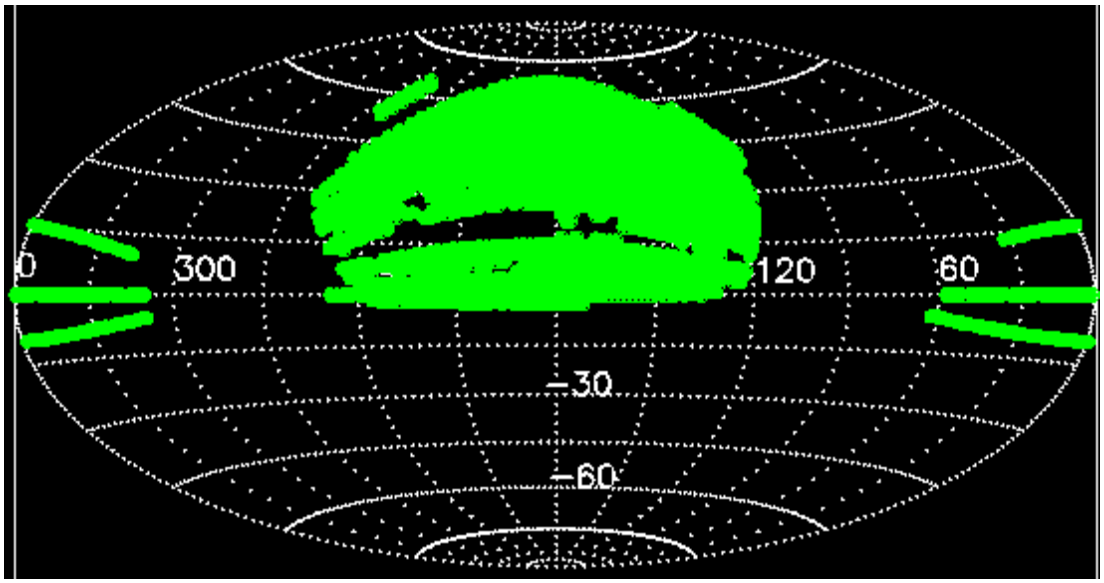

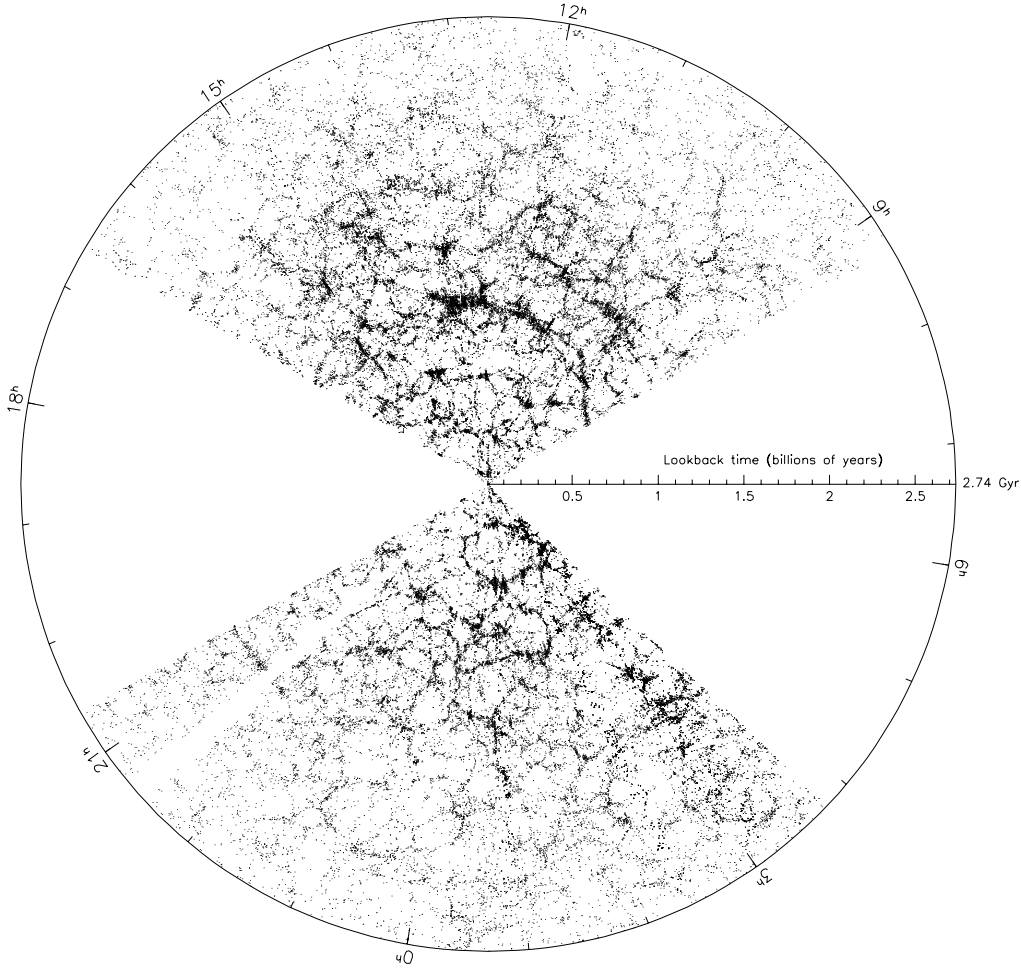

Fig. 4.— Zoom in of the region marked by the dotted circle in figure 3, showing SDSS galaxies out to 0.2 $t_{\rm horizon}$. The details of galaxy clustering are now displayed much better. However, like figure 2, it still fails to capture the whole survey in one, reasonably sized, map.

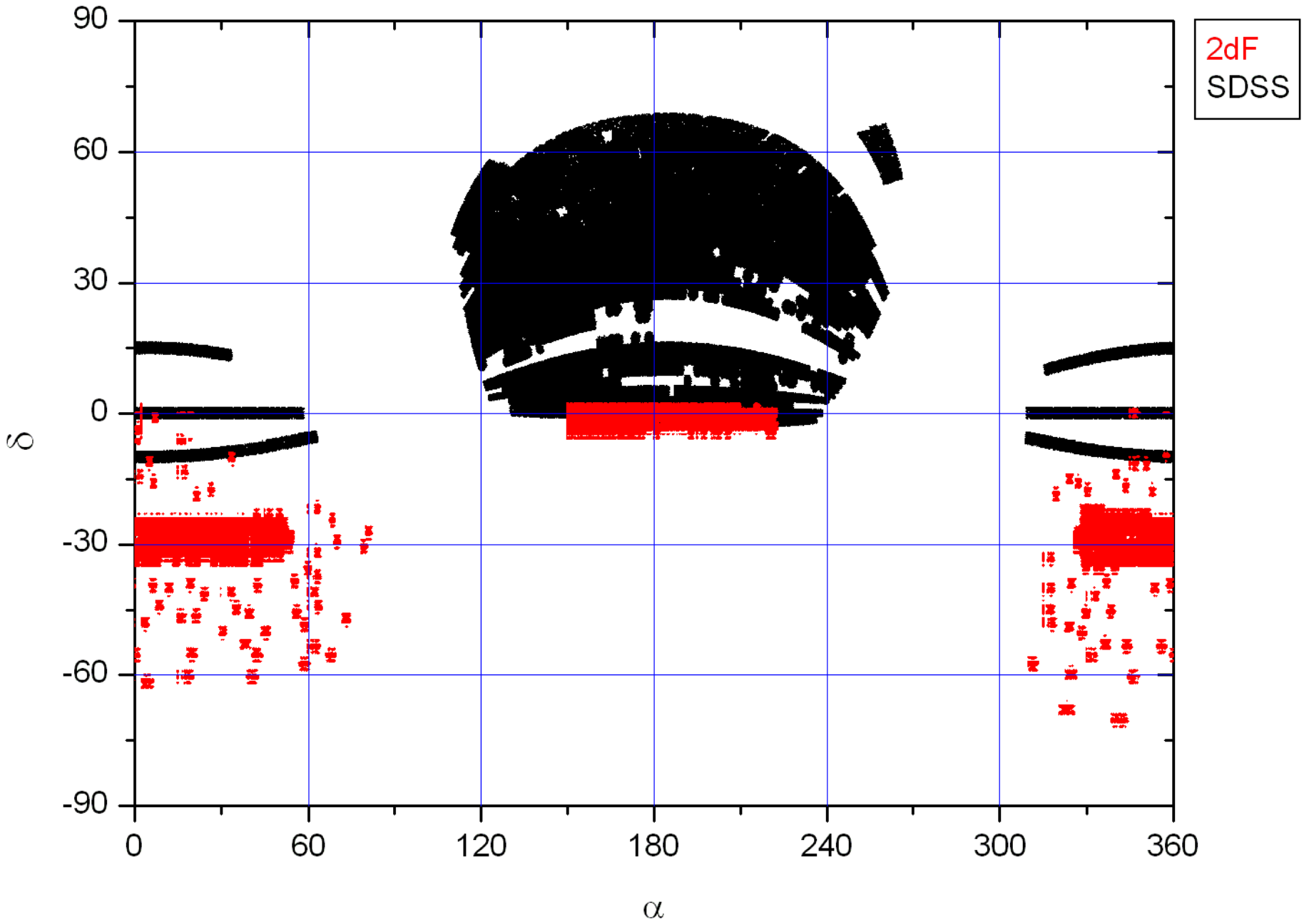
2dF & SDSS
2dF
SDSS
90
60
30
0
-30
-60
-90
δ
0
60
120
180
240
300
360
α

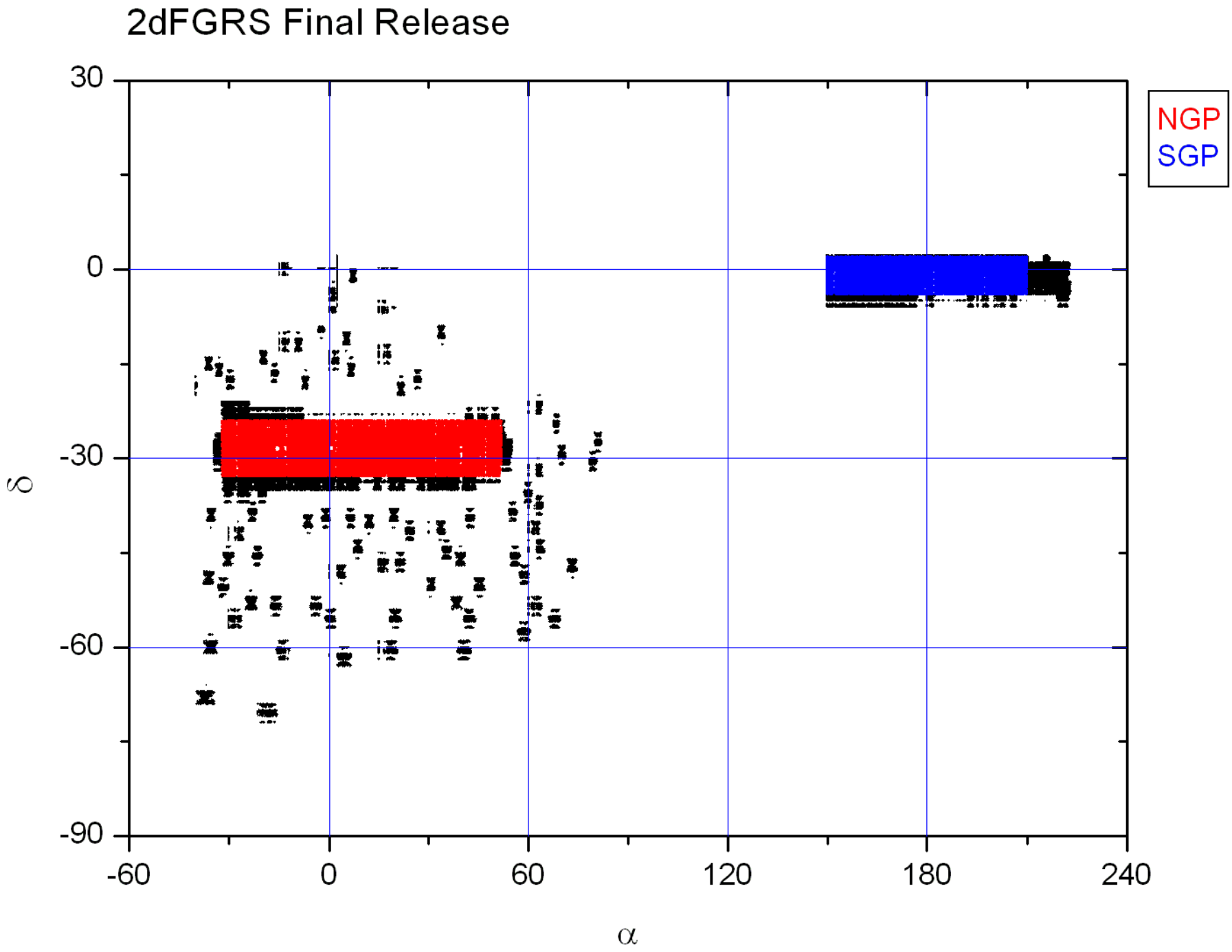
2dFGRS Final Release
30
0
-30
-60
-90
δ
-60
0
60
120
180
240
α
NGP
SGP

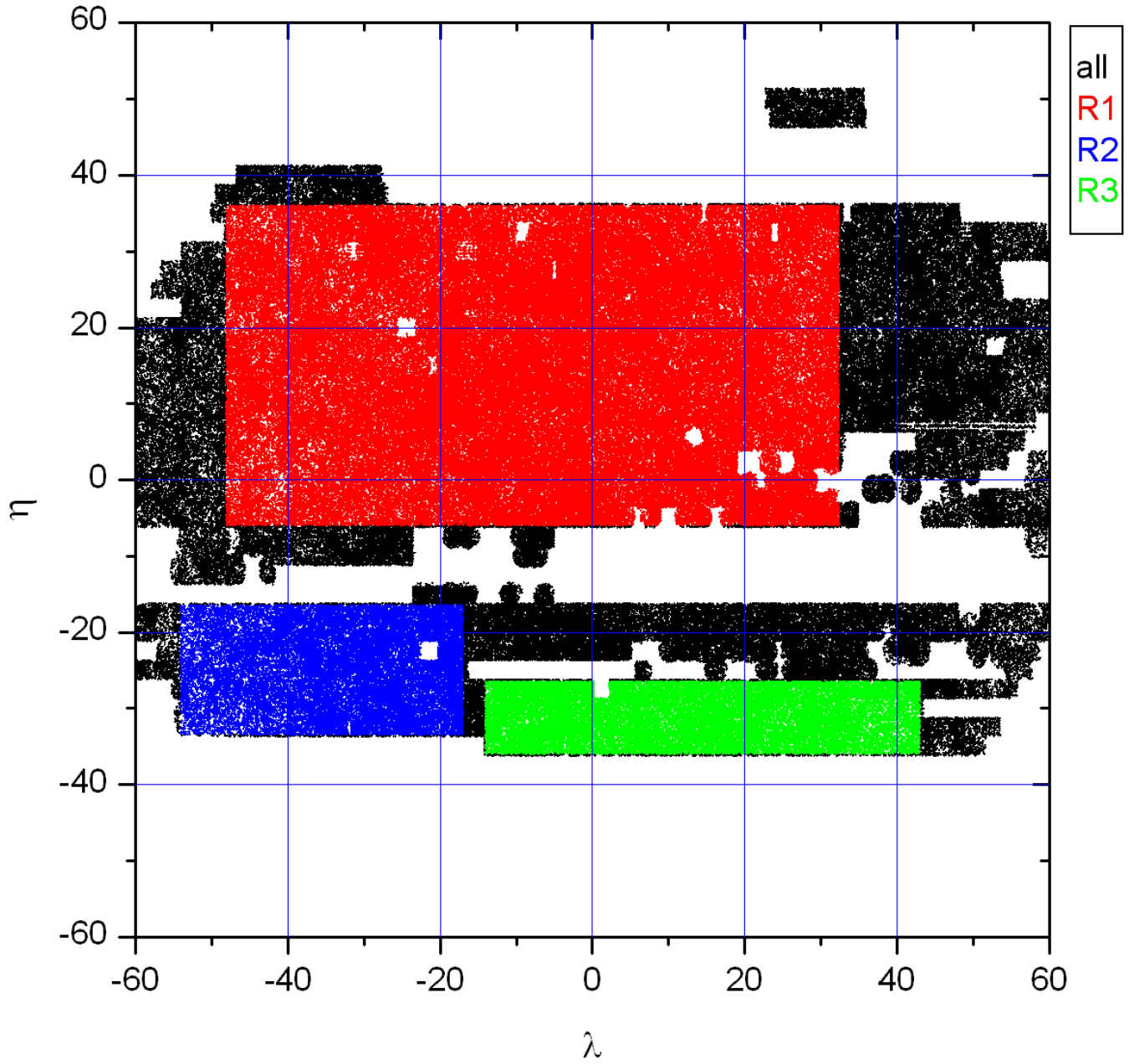
SDSS DR6 Main Galaxies
all
R1
R2
R3
60
40
20
0
-20
-40
-60
η
-60
-40
-20
0
20
40
60
λ

Metric distance

$$r(z) = \frac{c}{H_0} \int_{\frac{1}{1+z}}^{1} \frac{dy}{y \cdot \left(\Omega_M / y + \Omega_\Lambda \cdot y^2\right)^{1/2}},$$

$$\Omega_M = 0.3,\ \Omega_\Lambda = 0.7,\ H_0 = 100\ km \cdot s^{-1} \cdot Mpc^{-1}$$

Absolute magnitude

$$M = m - 5 \cdot \log_{10}\left[r(z) \cdot (1+z)\right] - K(z) - E(z) - 25$$

Apparent magnitudes and corrections

	2dFGRS	SDSS MG	SDSS LRG
Apparent magnitude band	b_J	r	g
Extinction correction	already corrected in catalog		
K-correction	Madgwick D. S., Lahav O. et al. 2002, MNRAS, 333, 133	Blanton et al., 2005, AJ, 129, 2562, http://sdss.physics.nyu.edu/vagc/	
E-correction	–	–	–

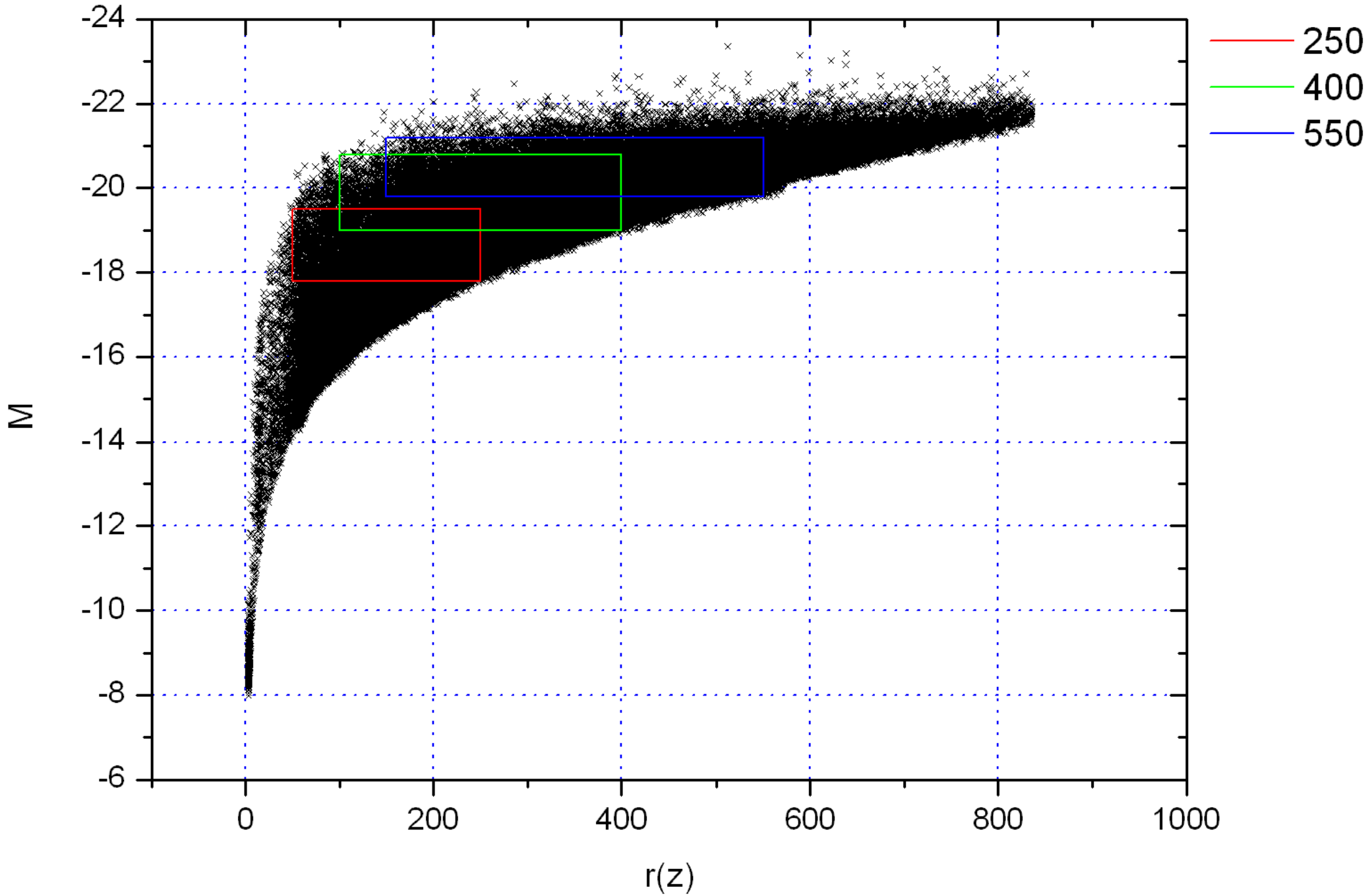
-24
-22
-20
-18
-16
-14
-12
-10
-8
-6
M
0
200
400
600
800
1000
r(z)
250
400
550

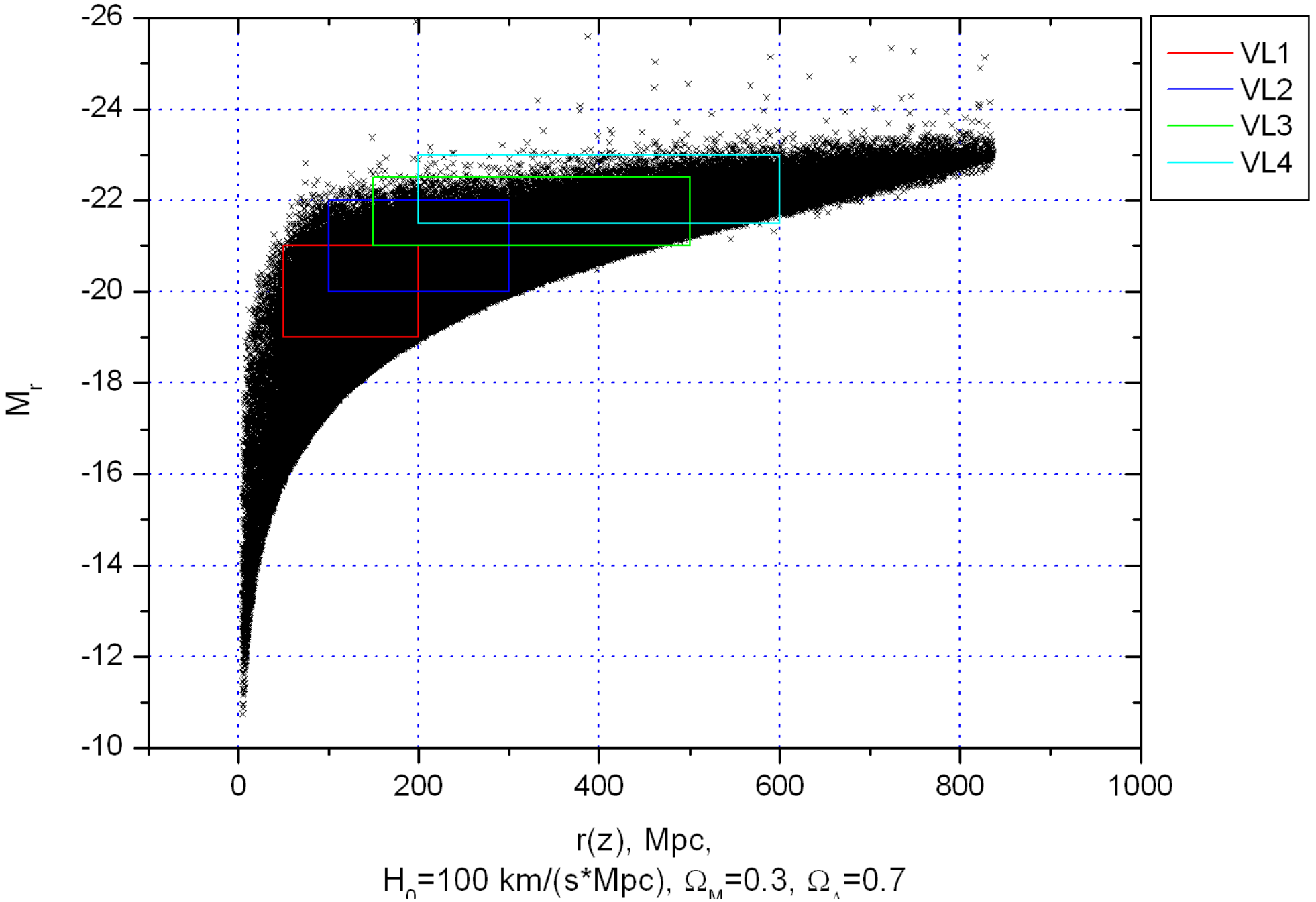
-26
-24
-22
-20
-18
-16
-14
-12
-10
M_r
0
200
400
600
800
1000
r(z), Mpc,
H_0=100 km/(s*Mpc), Ω_M=0.3, Ω_Λ=0.7
VL1
VL2
VL3
VL4

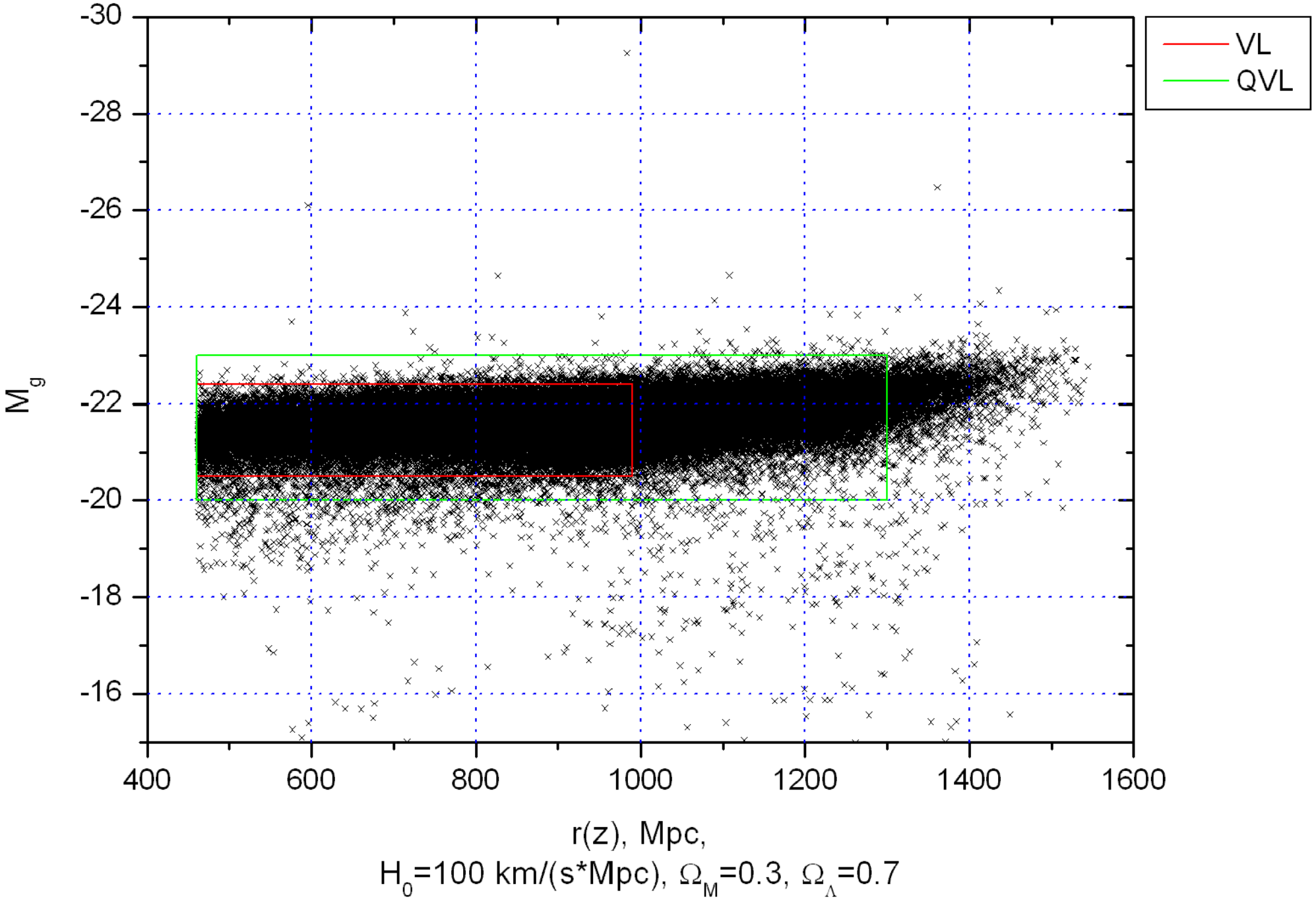
VL
QVL
-30
-28
-26
-24
-22
-20
-18
-16
M_g
400
600
800
1000
1200
1400
1600
r(z), Mpc,
H_0=100 km/(s*Mpc), Ω_M=0.3, Ω_Λ=0.7

VL sample	$r_{\min}$	$r_{\max}$	$M_{\min}$	$M_{\max}$	Ω	N_g
SGP250	50	250	-19.5	-17.8	0.20	14177
SGP400	100	400	-20.8	-19.0	0.20	29373
SGP550	150	550	-21.2	-19.8	0.20	26289
NGP250	50	250	-19.5	-17.8	0.11	12474
NGP400	100	400	-20.8	-19.0	0.11	23208
NGP550	150	550	-21.2	-19.8	0.11	18030

Table 1. Properties of the 2dFRGS VL samples: $r_{\min}$ and $r_{\max}$ are the chosen limits for the metric distance; $M_{\min}$ and $M_{\max}$ are the corresponding limits for the absolute magnitude; Ω is the solid angle of a region in steradians; N_g – the resulting number of galaxies in each subsample.

Region	$\eta_{\min}$	$\eta_{\max}$	$\lambda_{\min}$	$\lambda_{\max}$	Ω
R1	-48.0	32.5	-6.0	36.0	0.94
R2	-54.0	-17.0	-33.5	-16.5	0.15
R3	-14.0	43.0	-36.0	-26.5	0.15

Table 2. Properties of the angular regions considered for the SDSS: the limits (in degrees) are chosen using the intrinsic coordinates of the survey (η, λ); Ω is the solid angle of each region in steradians.

VL cut	$r_{\min}$	$r_{\max}$	$M_{\min}$	$M_{\max}$
MG1	50	200	-21.0	-19.5
MG2	100	300	-22.0	-20.0
MG3	150	500	-22.5	-21.0
MG4	200	600	-23.0	-21.5
LRG	460	990	-22.4	-20.5

Table 3. Selected VL cuts for SDSS galaxies: $r_{\min}$ and $r_{\max}$ are the chosen limits for the metric distance; $M_{\min}$ and $M_{\max}$ are the corresponding limits for the absolute magnitude (r-band for MG1 – MG4 and g-band for LRG).

Region / VL cut	R1	R2	R3
MG1	33259	5435	3891
MG2	43394	8765	9256
MG3	51717	9153	9324
MG4	30532	5061	5020
LRG	27150	4440	3957

Table 4. Number of galaxies in each VL subsample extracted from SDSS.

Statistical methods for Large Scale Structure analysis

Reduced two-point correlation function $\xi(r) = \frac{\langle n(r) \rangle_P}{\langle n \rangle} - 1$	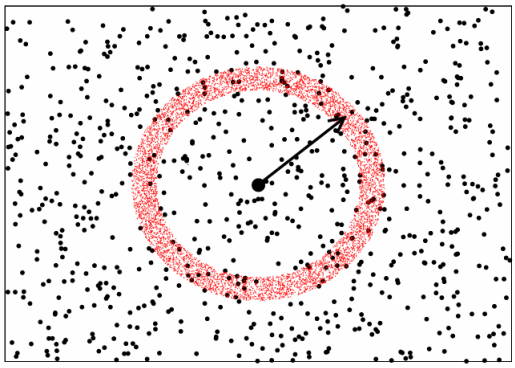 $\xi_{DP}(r) = \frac{N_R}{N_D - 1} \frac{DD(r)}{DR(r)} - 1$ $\xi_{LS}(r) = \frac{N_R(N_R - 1)}{N_D(N_D - 1)} \frac{DD(r)}{RR(r)} - 2\frac{N_R - 1}{N_D} \frac{DR(r)}{RR(r)} + 1$
Conditional density (in shells) $\Gamma(r) = \langle n(r) \rangle_P$	$\Gamma_E(r) = \frac{1}{N_C(r + \Delta r)} \sum_{i=1}^{N_C(r+\Delta r)} \frac{N_i(r, \Delta r)}{\|C(r, \Delta r)\|}$ $\xi_{FS}(r) = \frac{\Gamma_E(r)}{\bar{n}} - 1$
Integrated conditional density (in spheres) $\Gamma^*(r) = \langle n(r' < r) \rangle_P$	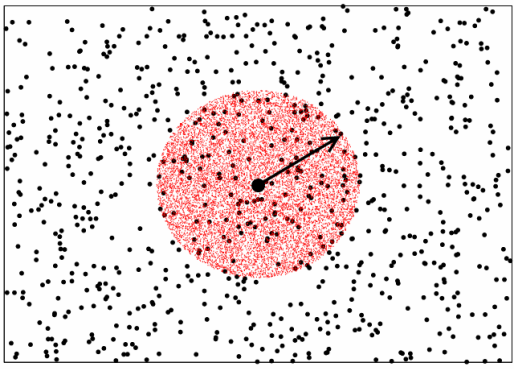 $\Gamma_E^*(r) = \frac{1}{N_C(r)} \sum_{i=1}^{N_C(r)} \frac{N_i(r)}{\|C(r)\|}$
Nearest neighbor probability density $\omega(r)$	$\omega_E(r) = N_{nn}(r) \Big/ \left(\int_0^\infty N_{nn}(r') dr' \right)$

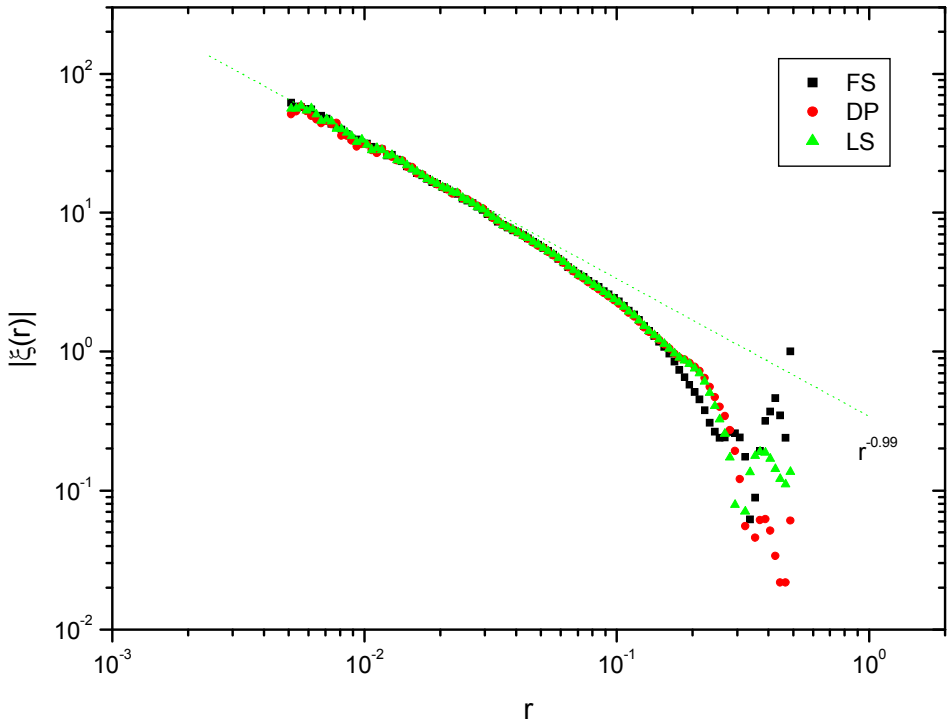

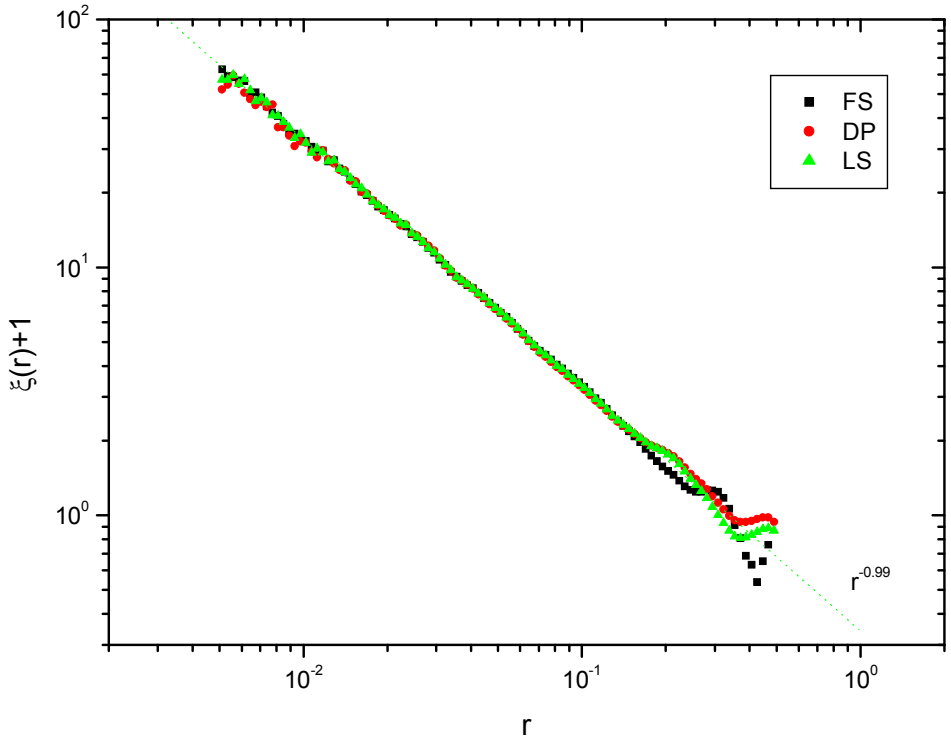

Random Cantor Set, 10^4 points, $D = 2$

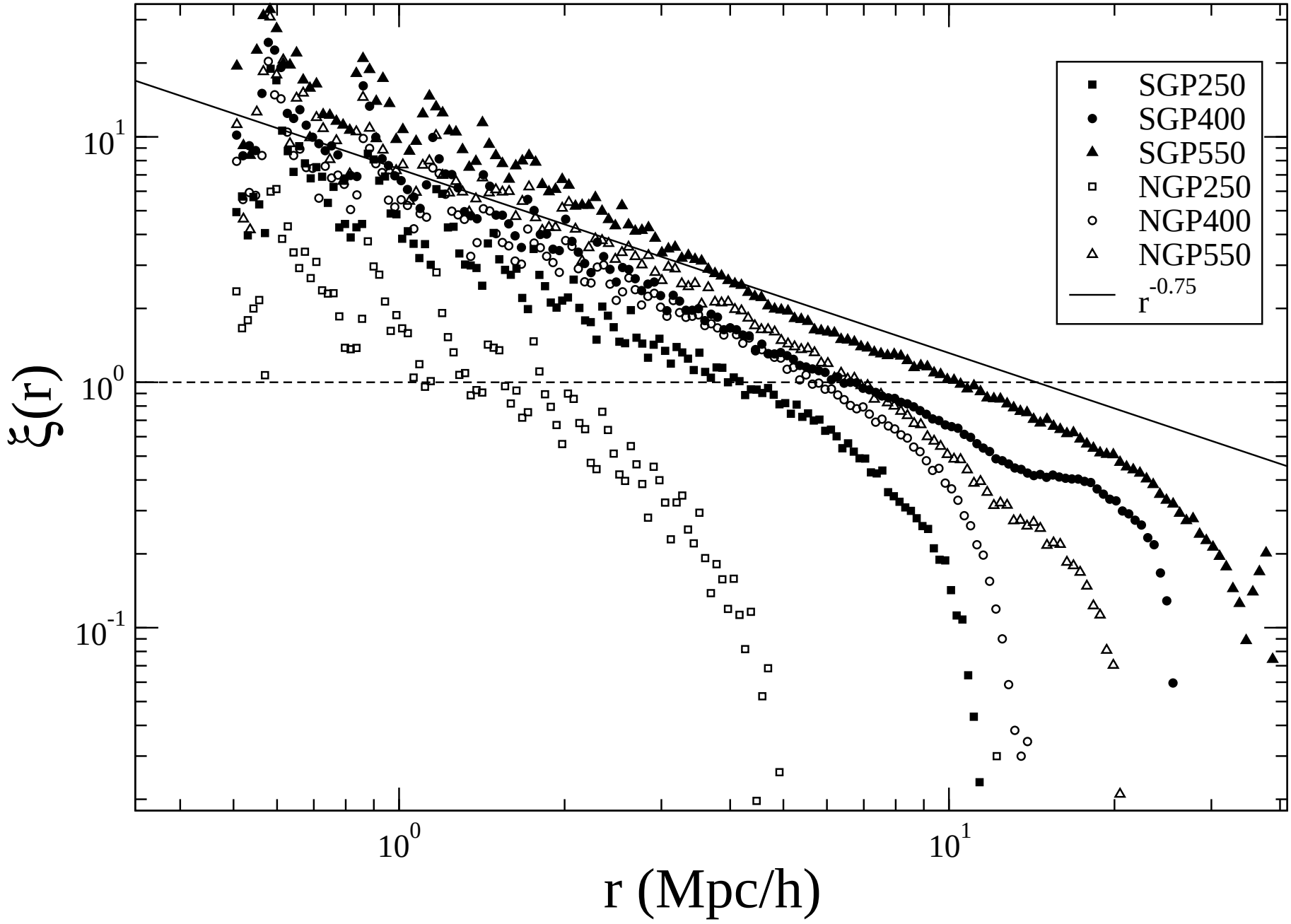
SGP250
SGP400
SGP550
NGP250
NGP400
NGP550
r^-0.75
ξ(r)
10^1
10^0
10^-1
10^0
10^1
r (Mpc/h)

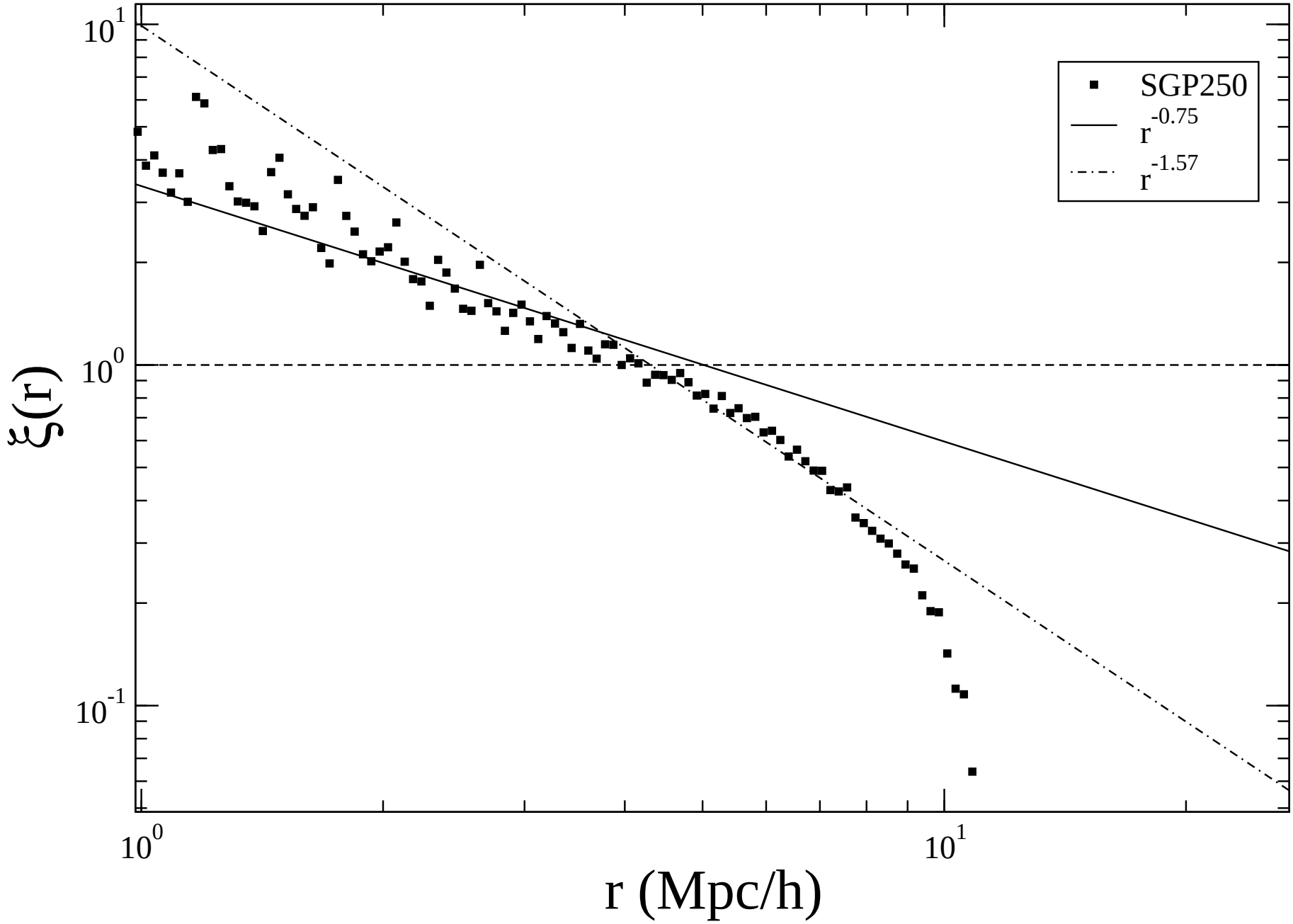
SGP250
r^-0.75
r^-1.57
ξ(r)
r (Mpc/h)
10^1
10^0
10^-1
10^0
10^1

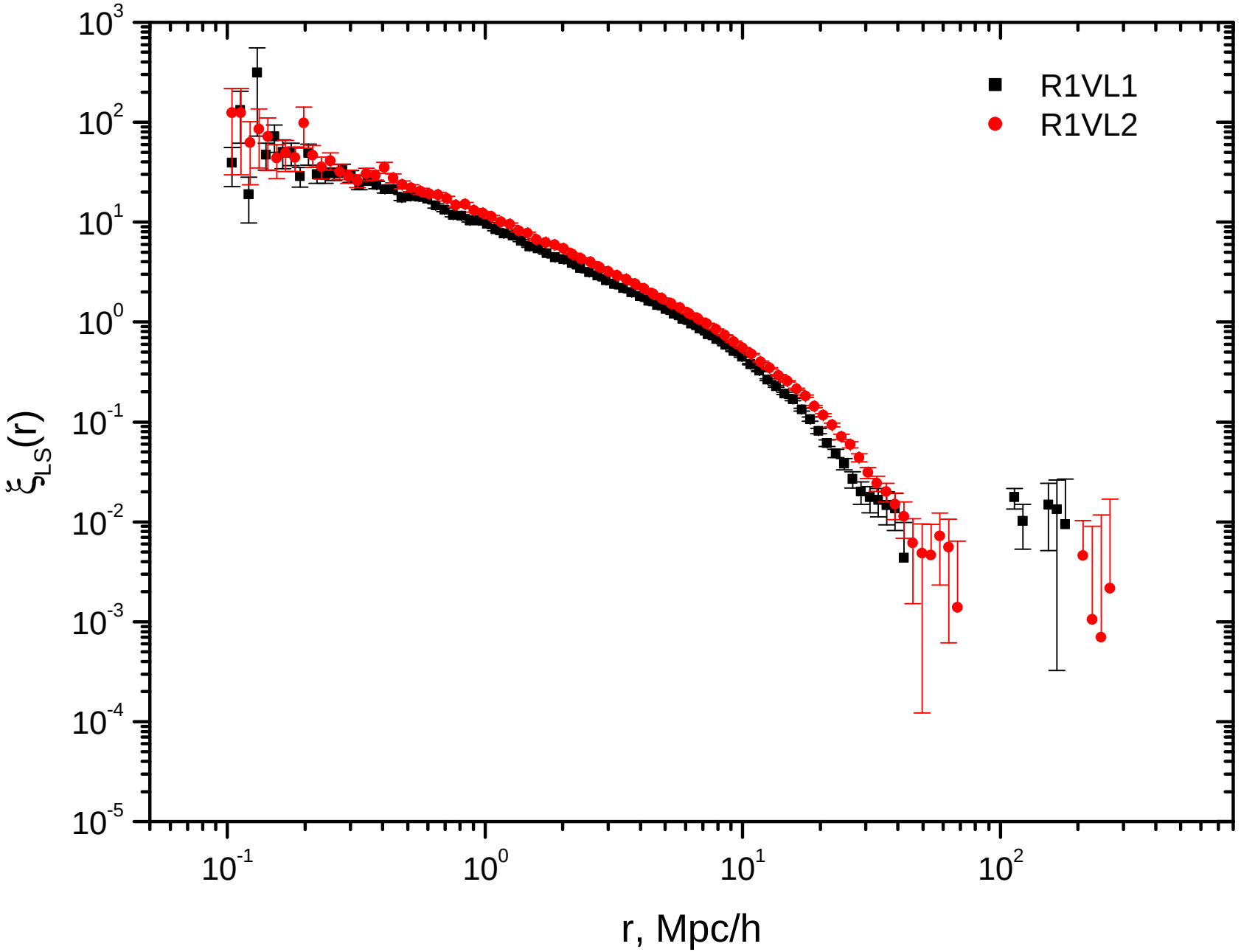
R1VL1
R1VL2
$\xi_{LS}(r)$
r, Mpc/h
10^{3}
10^{2}
10^{1}
10^{0}
10^{-1}
10^{-2}
10^{-3}
10^{-4}
10^{-5}
10^{-1}
10^{0}
10^{1}
10^{2}

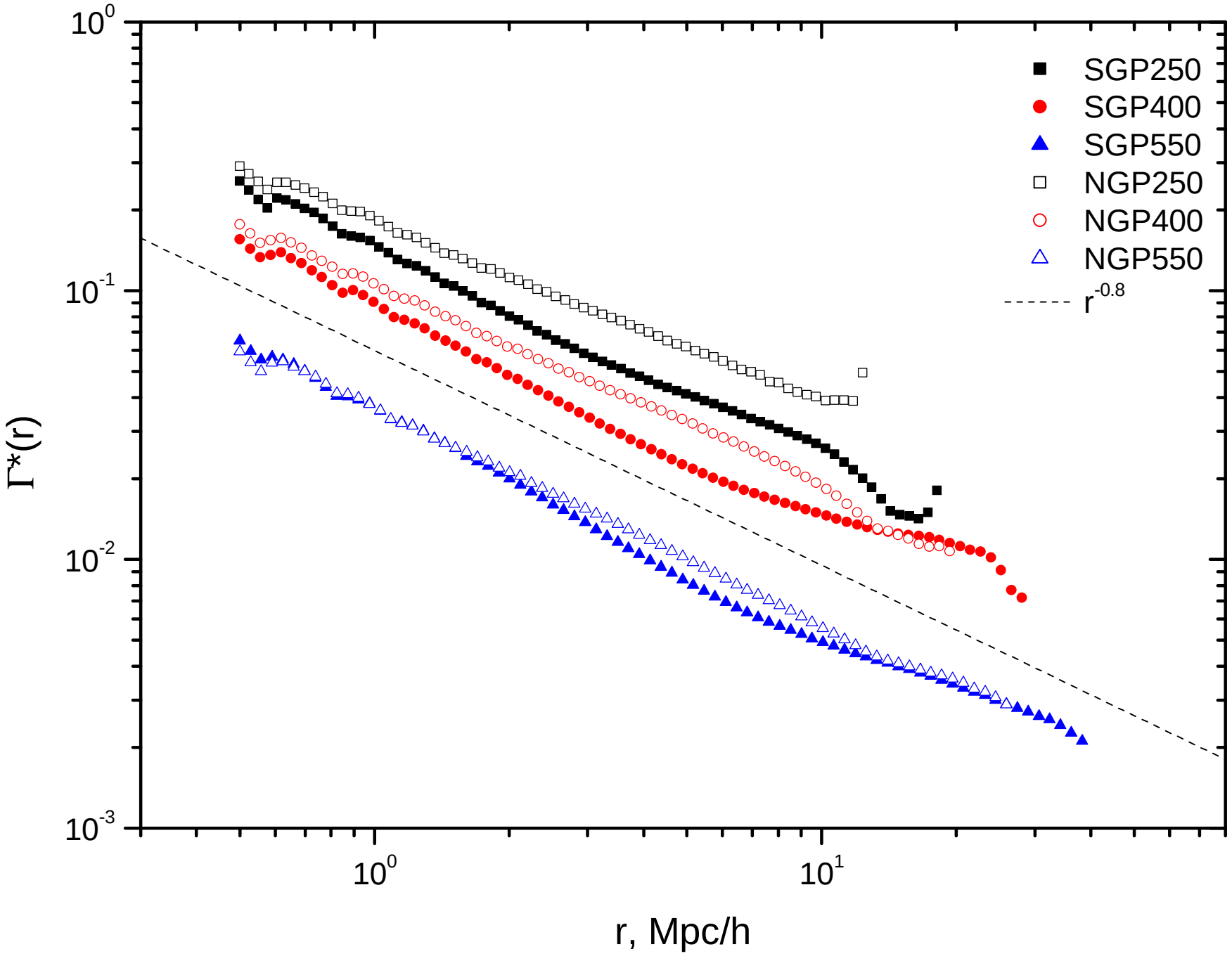
SGP250
SGP400
SGP550
NGP250
NGP400
NGP550
r^-0.8
Γ*(r)
r, Mpc/h
10^0
10^-1
10^-2
10^-3
10^0
10^1

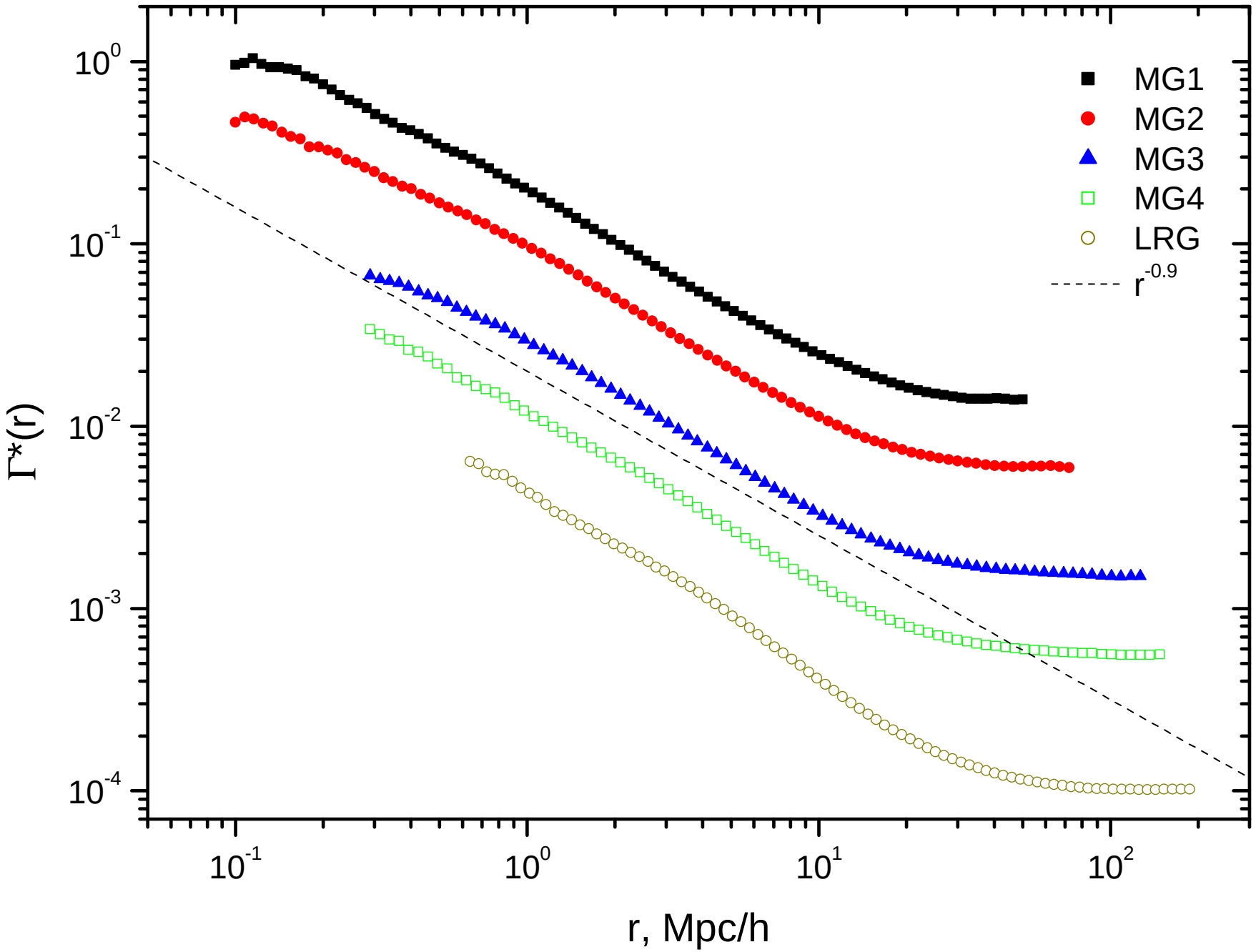
MG1
MG2
MG3
MG4
LRG
r^-0.9
Γ*(r)
r, Mpc/h
10^0
10^-1
10^-2
10^-3
10^-4
10^-1
10^0
10^1
10^2

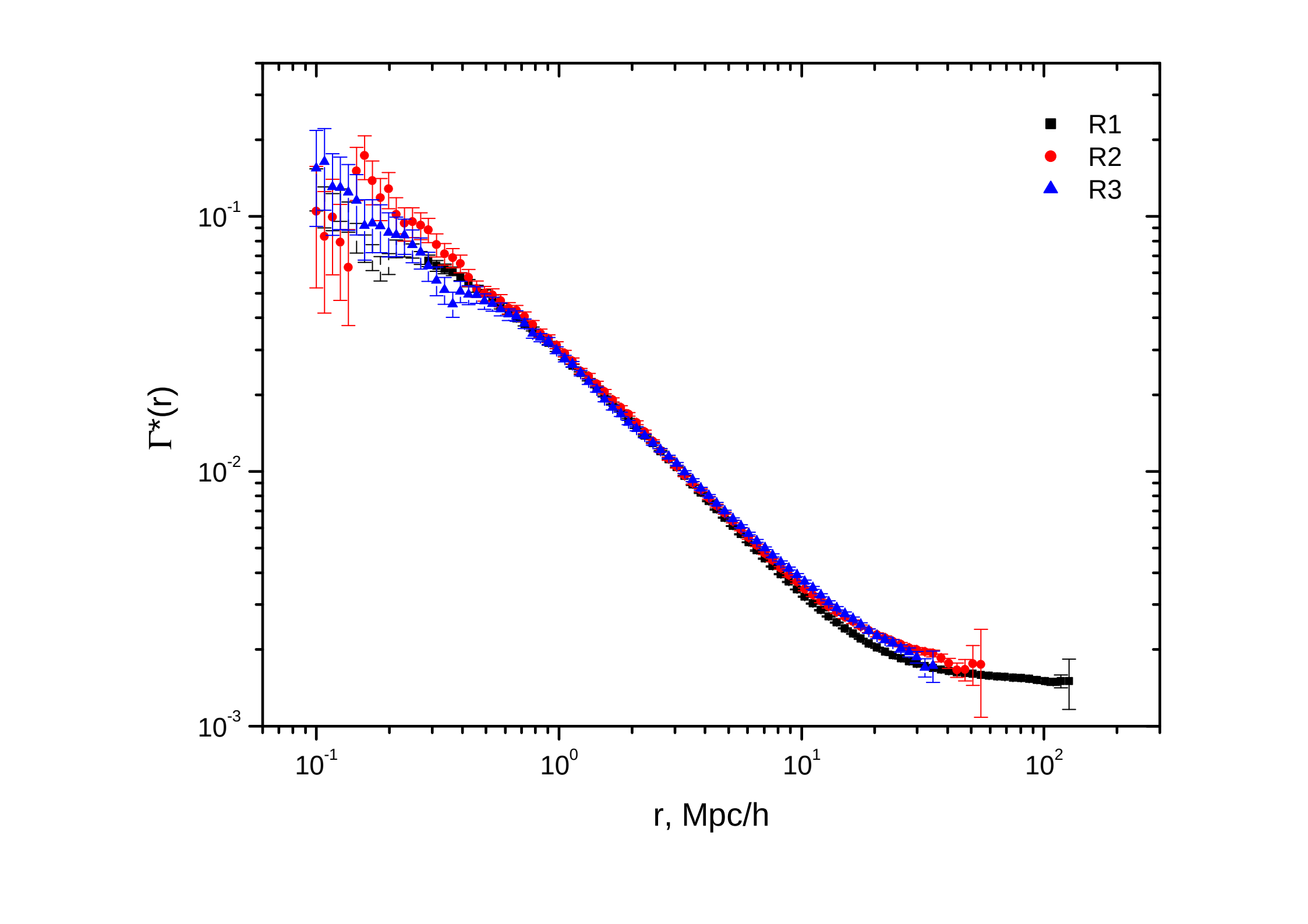
R1
R2
R3
Γ*(r)
r, Mpc/h
10^-1
10^-2
10^-3
10^-1
10^0
10^1
10^2

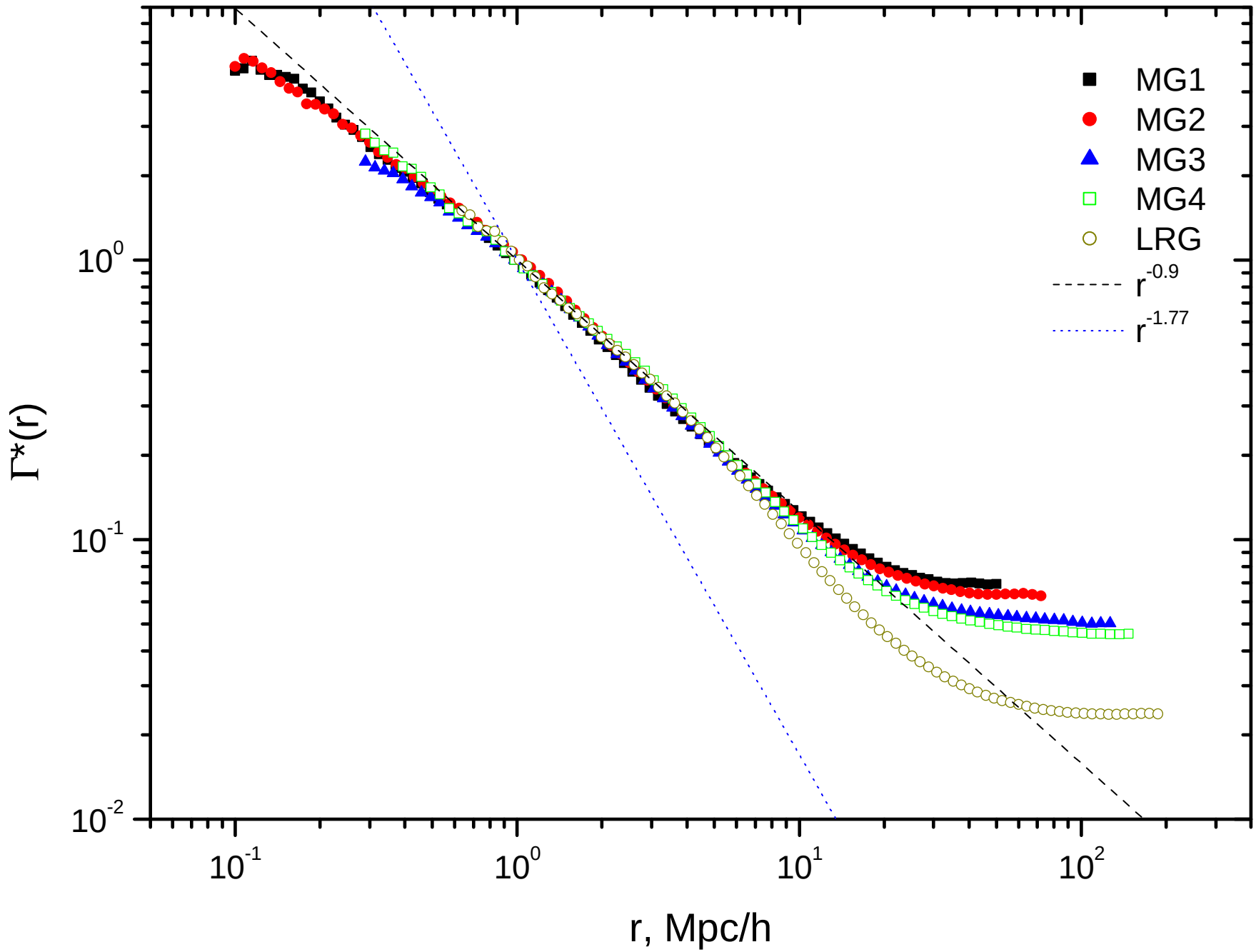
MG1
MG2
MG3
MG4
LRG
r^-0.9
r^-1.77
Γ*(r)
r, Mpc/h
10^0
10^-1
10^-2
10^-1
10^0
10^1
10^2

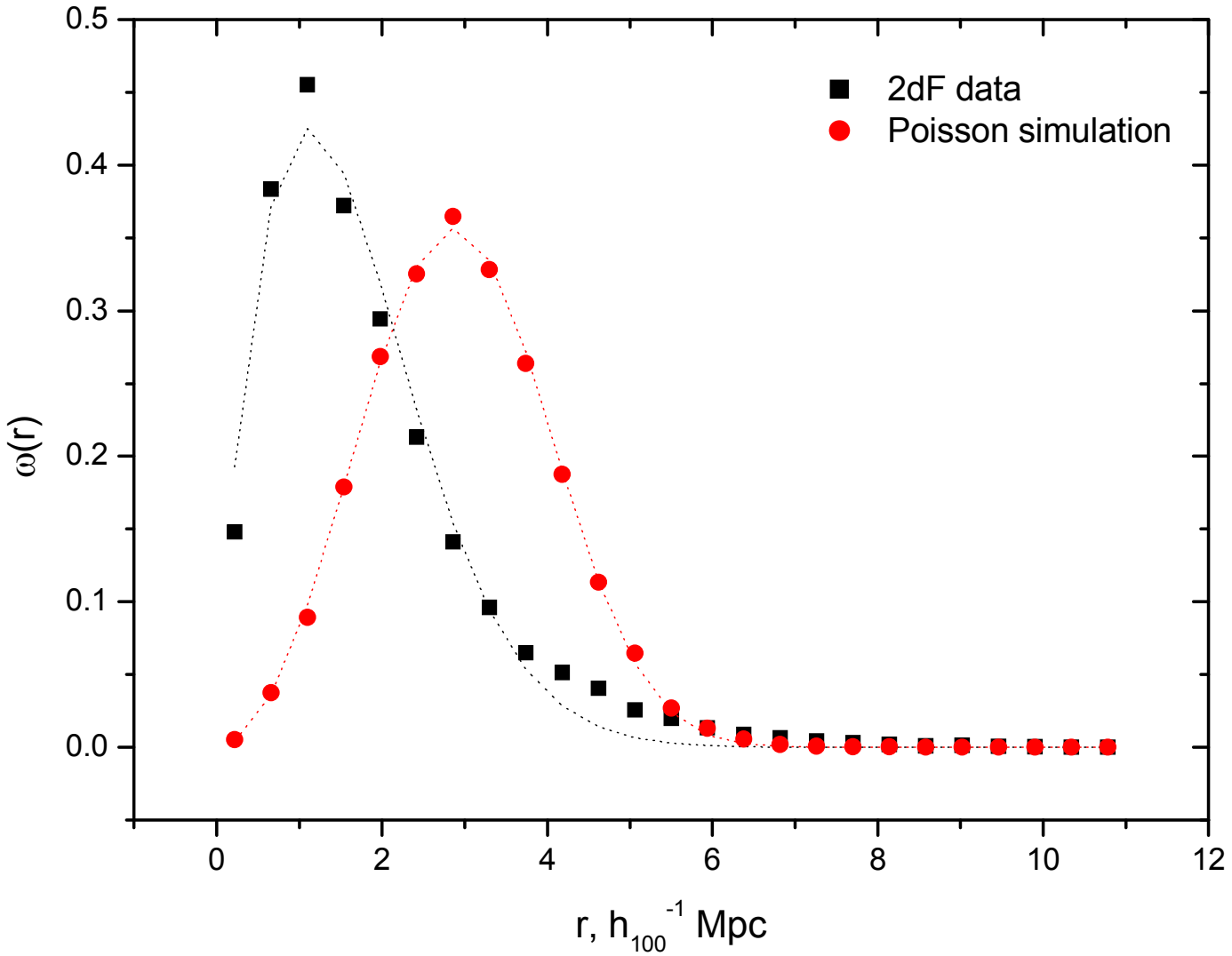

Poisson

$$\omega(r) = 4\pi\langle n\rangle r^2 \exp\left(-\frac{4\pi\langle n\rangle r^3}{3}\right)$$

Correlated

$$\omega(r) = 4\pi C r^{2-\gamma} \exp\left(-\frac{4\pi C}{3-\gamma} r^{3-\gamma}\right)$$

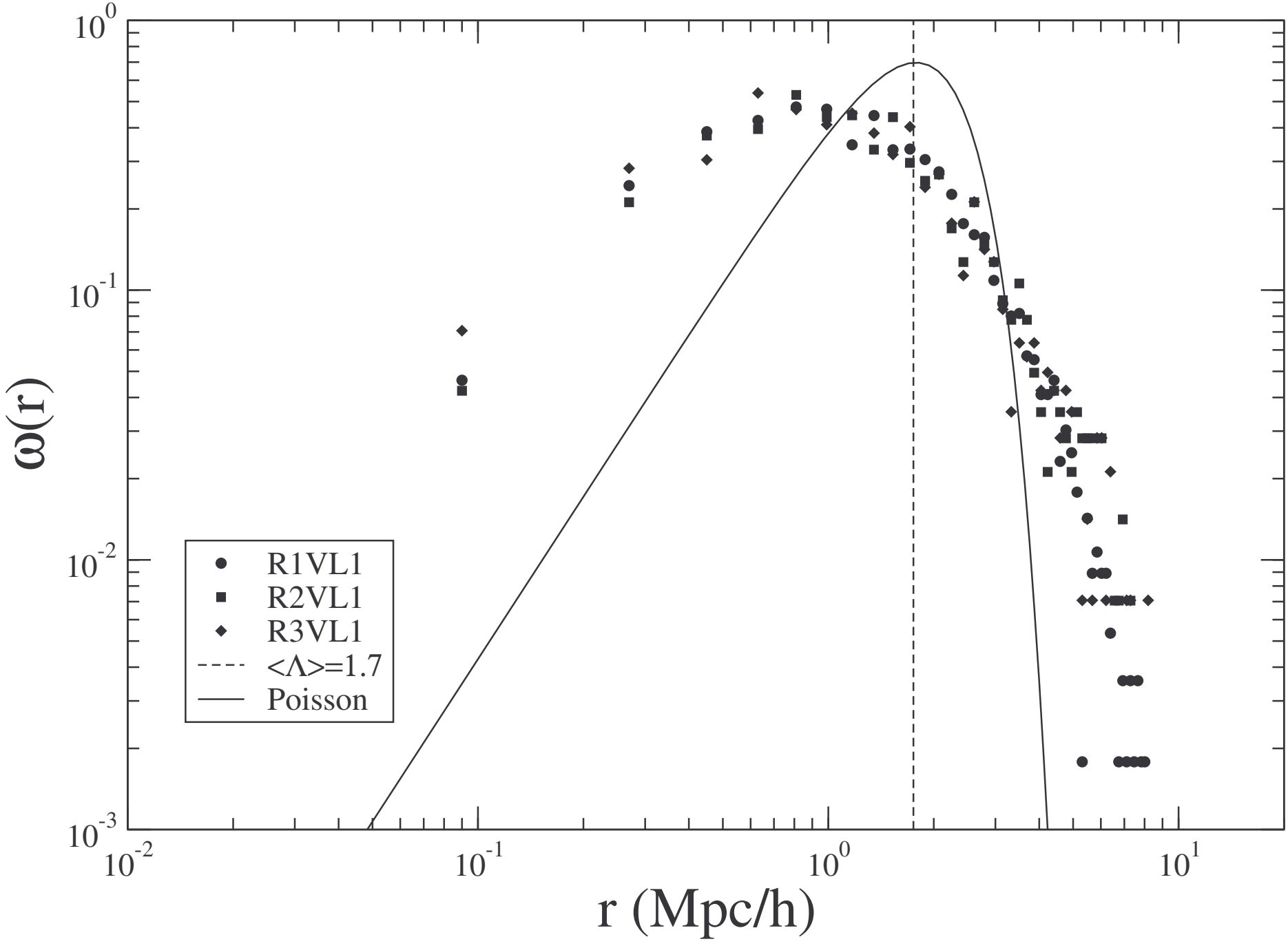
10^0
10^{-1}
10^{-2}
10^{-3}
10^{-2}
10^{-1}
10^0
10^1
ω(r)
r (Mpc/h)
R1VL1
R2VL1
R3VL1
<Λ>=1.7
Poisson

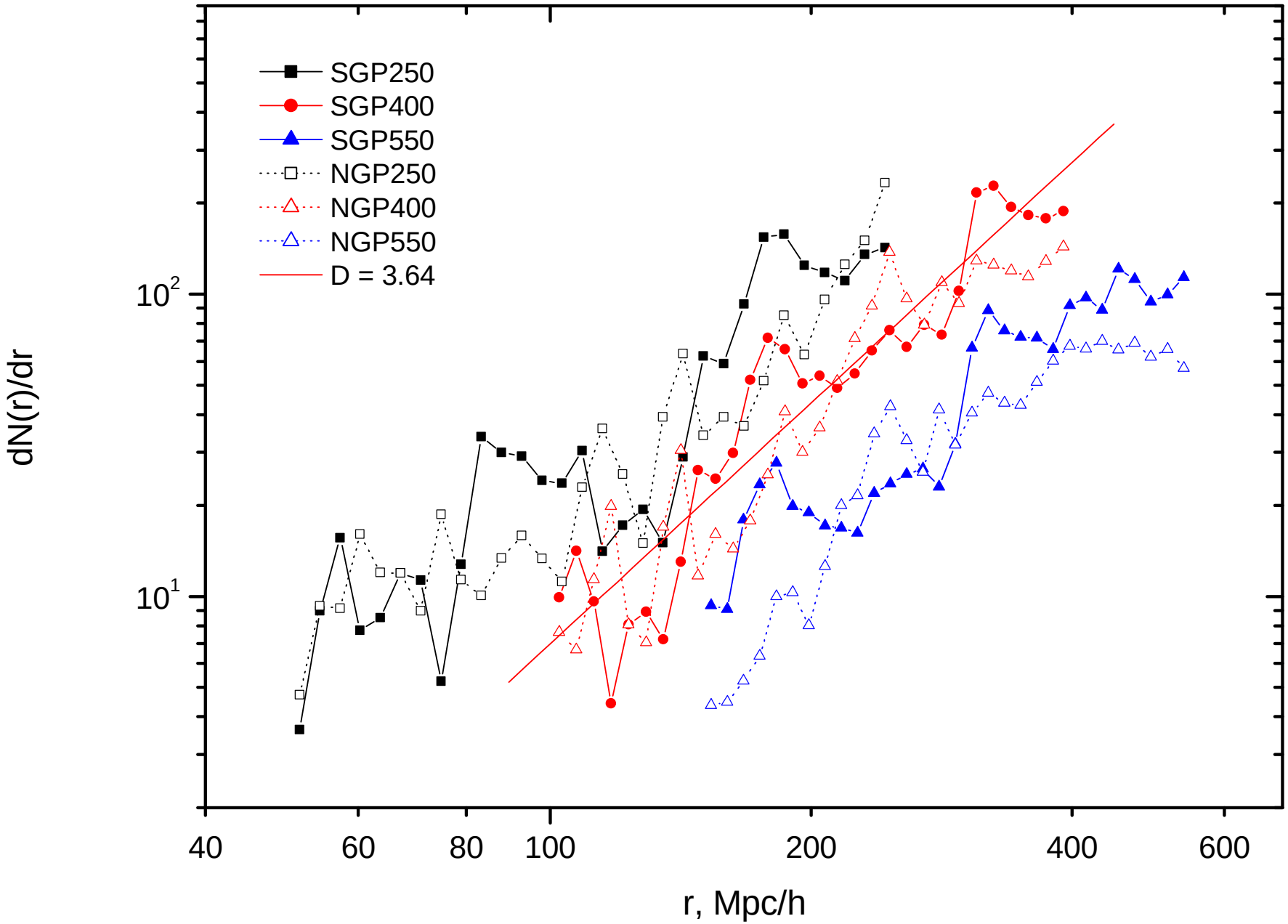
SGP250
SGP400
SGP550
NGP250
NGP400
NGP550
D = 3.64
dN(r)/dr
10^2
10^1
40
60
80
100
200
400
600
r, Mpc/h

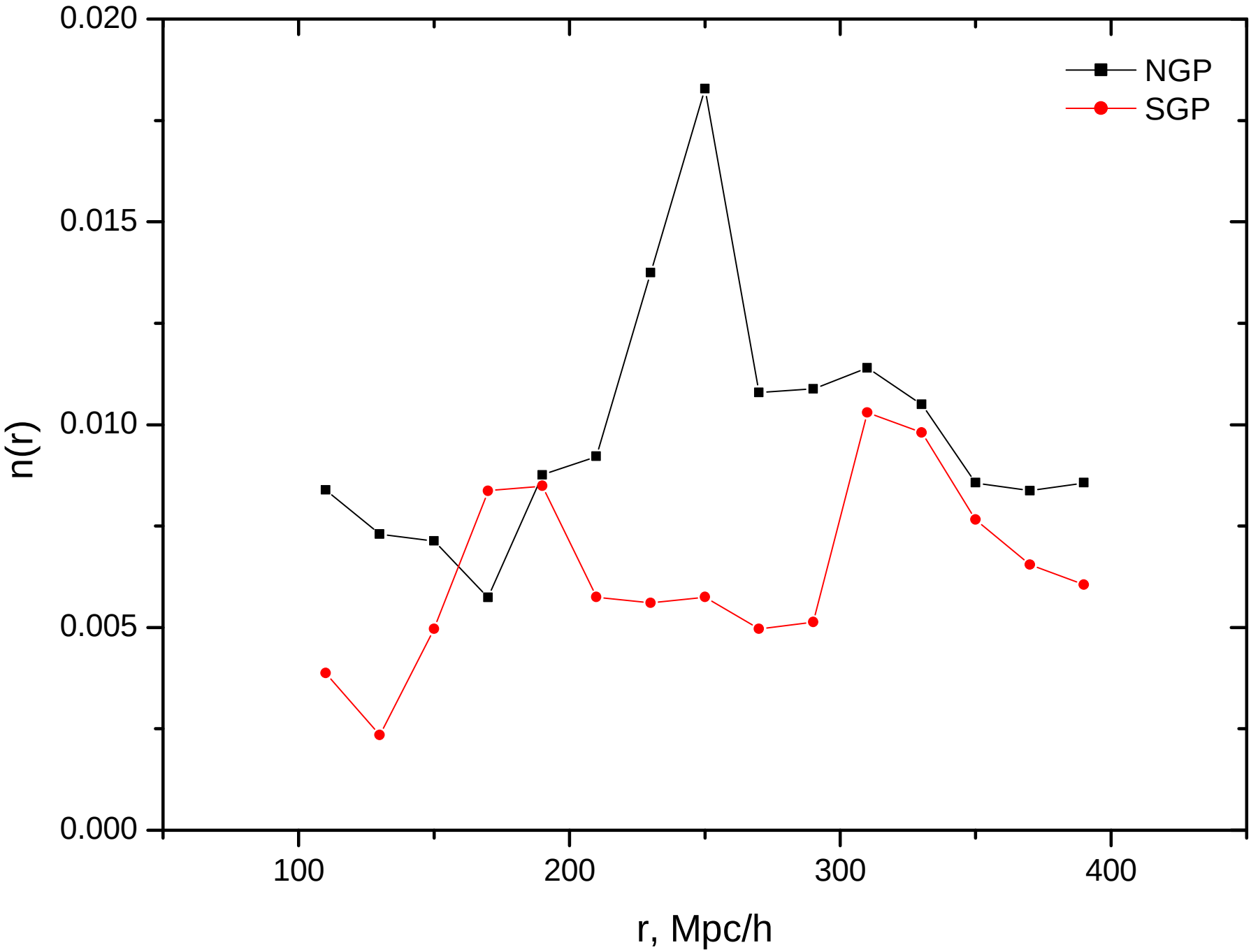
0.020
0.015
0.010
0.005
0.000
n(r)
100
200
300
400
r, Mpc/h
NGP
SGP

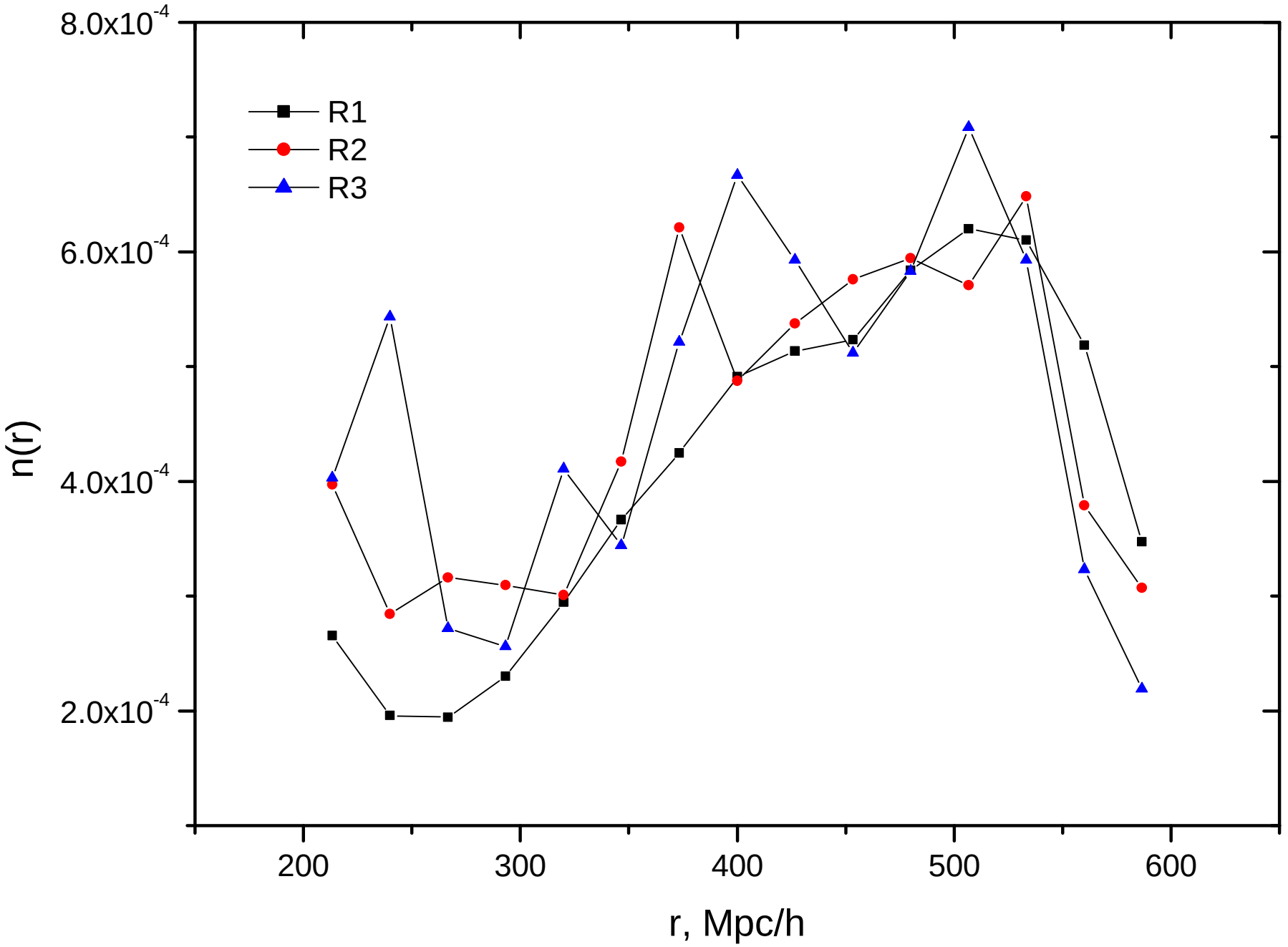
8.0x10-4
6.0x10-4
4.0x10-4
2.0x10-4
n(r)
R1
R2
R3
200
300
400
500
600
r, Mpc/h

Conclusions

- ✓ Correlation analysis of 2dFGRS shows that conditional density (not reduced correlation function) has a power-law behavior with exponent $\gamma = 0.8 \pm 0.2$ ($\mathrm{D} = 2.2 \pm 0.2$) in a range $1.0 < r < 40h^{-1}$ Mpc
- ✓ Correlation analysis of SDSS DR6 shows that
  - o Conditional density has a power-law behavior with exponent $\gamma = 0.9 \pm 0.1$ ($\mathrm{D} = 2.1 \pm 0.1$) in a range $0.5 < r < 30h^{-1}$ Mpc
  - o There is a crossover towards flat regime in a range $30 < r < 100h^{-1}$ Mpc (depends on sample depth), which can be interpreted as homogeneity
- ✓ There is no strong dependency of the power-law exponent on the luminosity of galaxies
- ✓ There are strong evidences of the super-large scale structures or selection effects with the samples being analyzed (shown by number counts and radial density function)
- ✓ Several important parameters should be controlled to verify reliability of the results
  - o Maximum full sphere radius $r_{sph}^{\max}$, average separation distance between nearest neighbors r_{sep}
  - o Number of full spheres for a given radius, degree of intersections between spheres
- ✓ We still need better statistics (larger solid angle and sample depth) to precisely identify the scales where crossover towards homogeneity occurs (and samples become transitionally invariant)

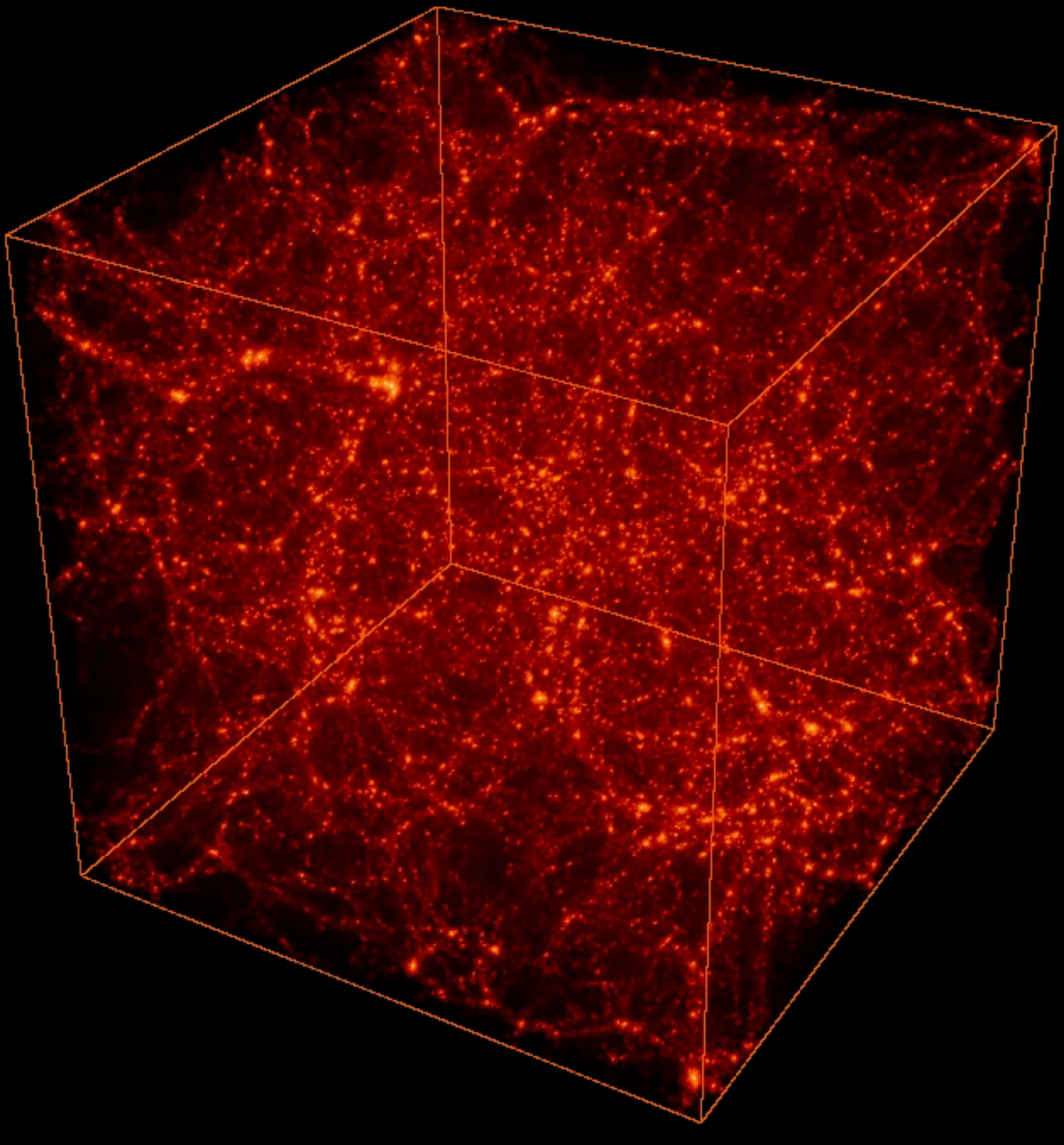

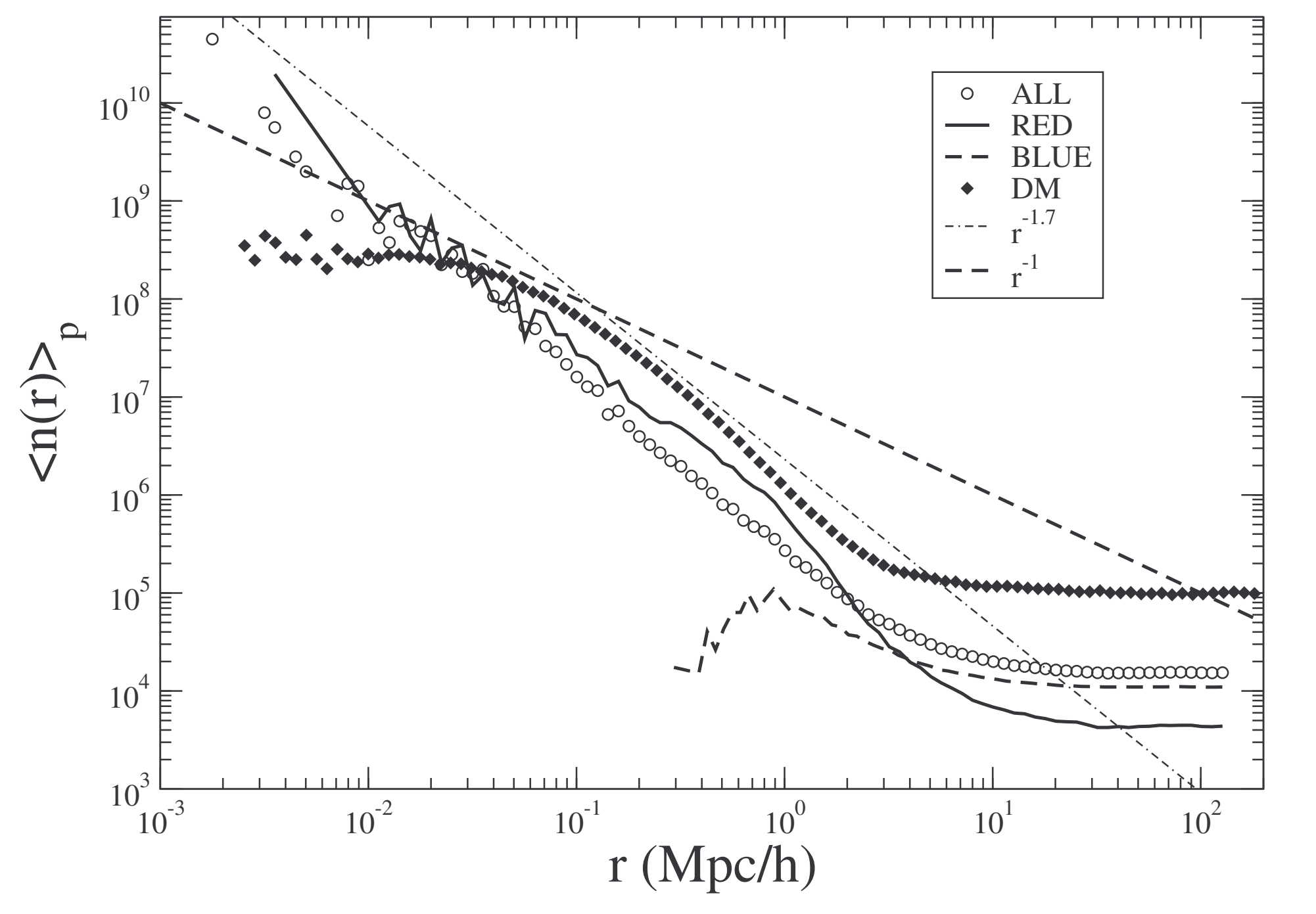
ALL
RED
BLUE
DM
r^-1.7
r^-1
<n(r)>_p
r (Mpc/h)
10^10
10^9
10^8
10^7
10^6
10^5
10^4
10^3
10^-3
10^-2
10^-1
10^0
10^1
10^2

CROSS-CORRELATION WEAK LENSING OF SDSS GALAXY CLUSTERS II: CLUSTER DENSITY PROFILES AND THE MASS–RICHNESS RELATION

David E. Johnston,[1,2] Erin S. Sheldon,[3] Risa H. Wechsler,[8] Eduardo Rozo,[9] Benjamin P. Koester, [4,11] Joshua A. Frieman,[4,10,11] Timothy A. McKay,[5,6,7] August E. Evrard,[5,6,7] Matthew R. Becker [5] James Annis, [10]

(Received; Accepted)
Draft version February 1, 2008

ABSTRACT

We interpret and model the statistical weak lensing measurements around 130,000 groups and clusters of galaxies in the Sloan Digital Sky Survey presented by Sheldon et al. (2007). We present non-parametric inversions of the 2D shear profiles to the mean 3D cluster density and mass profiles in bins of both optical richness and cluster *i*-band luminosity. Since the mean cluster density profile is proportional to the cluster–mass correlation function, the mean profile is spherically symmetric by the assumptions of large-scale homogeneity and isotropy. We correct the inferred 3D profiles for systematic effects, including non-linear shear and the fact that cluster halos are not all precisely centered on their brightest galaxies. We also model the measured cluster shear profile as a sum of contributions from the brightest central galaxy, the cluster dark matter halo, and neighboring halos. We infer the relations between mean cluster virial mass and optical richness and luminosity over two orders of magnitude in cluster mass; the virial mass at fixed richness or luminosity is determined with a precision of $\sim 13\%$ including both statistical and systematic errors. We also constrain the halo concentration parameter and halo bias as a function of cluster mass; both are in good agreement with predictions from N-body simulations of LCDM models. The methods employed here will be applicable to deeper, wide-area optical surveys that aim to constrain the nature of the dark energy, such as the Dark Energy Survey, the Large Synoptic Survey Telescope and space-based surveys.

Subject headings: gravitational lensing – galaxies: clusters – large-scale structure – cosmology:observations – galaxies: halos – dark matter

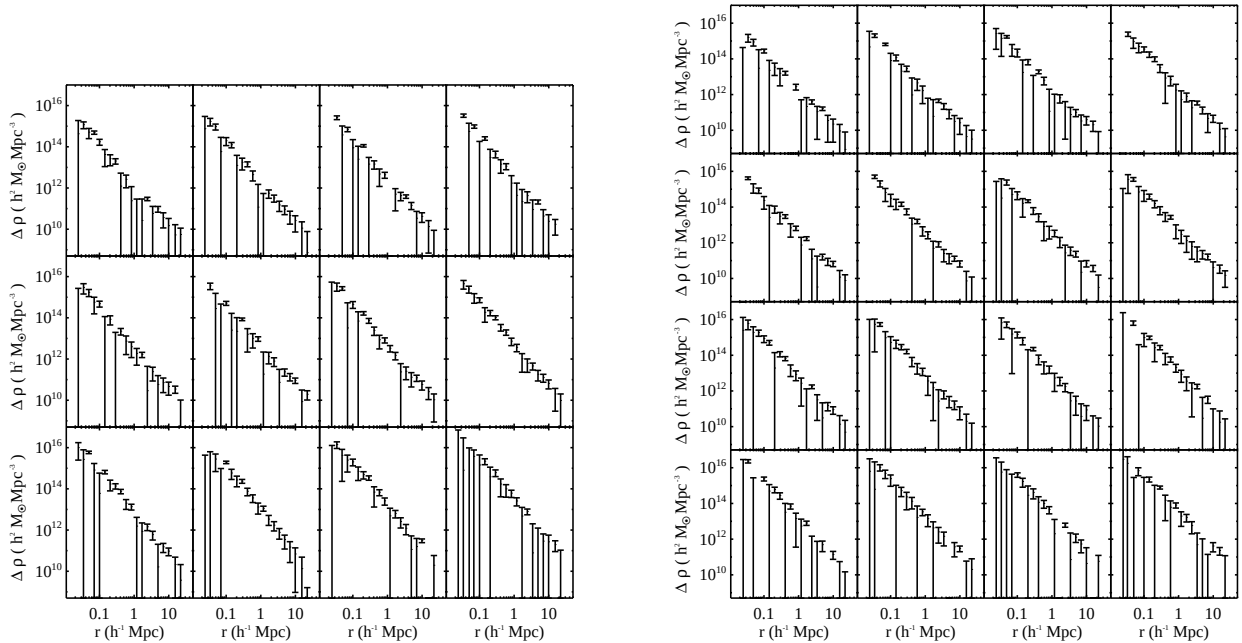

FIG. 2.— **Left:** Inverted mean density profiles, $\Delta\rho(r)$, for the 12 N_{200} richness bins shown in Fig. 1. **Right:** Inverted $\Delta\rho(r)$ profiles for the 16 L_{200} richness bins shown in Fig. 1.

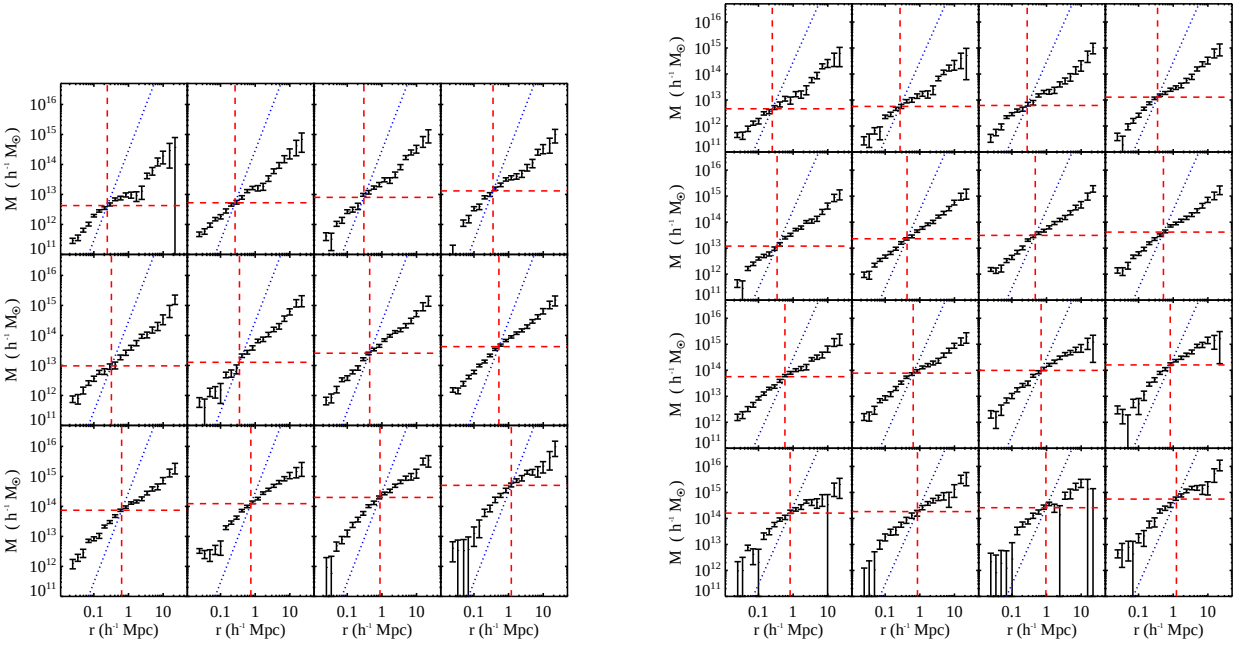

FIG. 3.— **Left:** Inverted 3D aperture mass profiles, $M(r)$, for the 12 N_{200} richness bins. The dotted blue diagonal line in each panel denotes 200 ρ_c 4/3 π r^3 (see Eqn. 4); this crosses the mass profile at r_{200} and M_{200}, which are indicated with the dashed red vertical and horizontal lines. **Right:** Inverted 3D aperture mass profiles, $M(r)$, for the 16 L_{200} richness bins.

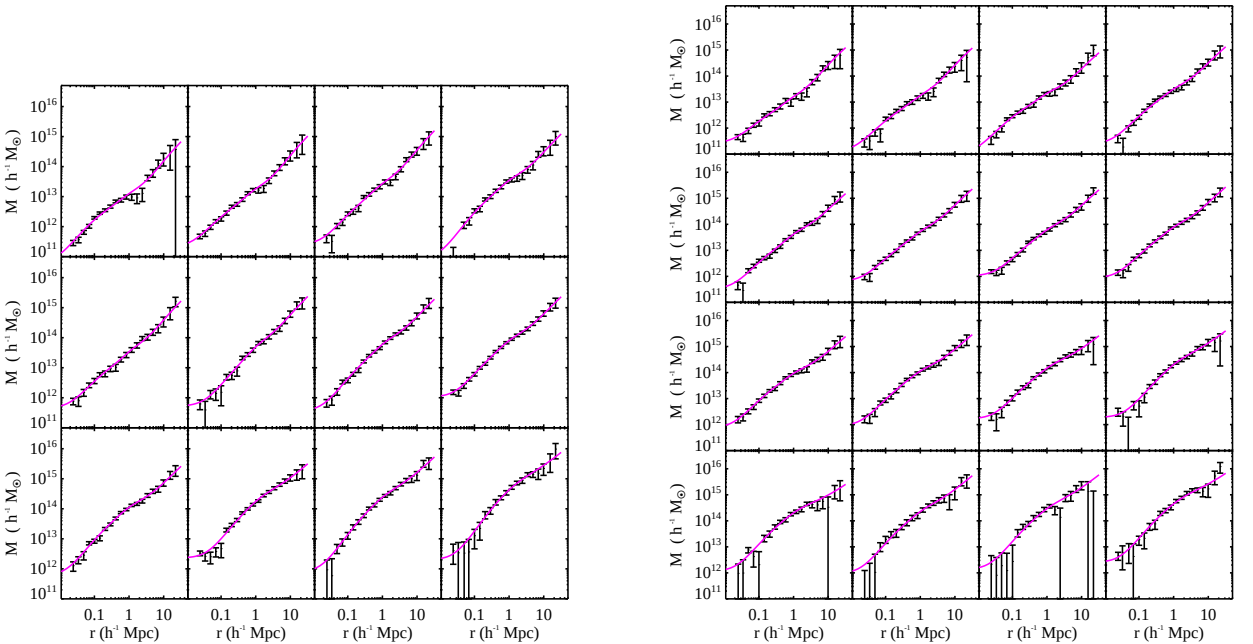

FIG. 10.— The model fits of Fig. 8 and 9 over-plotted on the inverted 3D mass profiles for the 12 N_{200} richness (*left panel*) and 16 L_{200} luminosity bins (*right panel*).